Solar Wind: the Legacy of Helios and the promises of Solar Orbiter

Raffaella D'Amicis
INAF-IAPS, Rome, Italy

Ground based and space instruments for
researches in Solar-Terrestrial Physics
6-10 June 2016, L'Aquila, Italy

Outline

- State of the art on solar wind observations (**Helios** data)
  - Solar wind and IMF macrostructure
  - Differences between fast and slow wind and radial evolution
- Open issues
- The upcoming **Solar Orbiter** mission

Helios program

Most of our knowledge about solar wind plasma and magnetic field in the inner heliosphere is due to Helios 1-2 s/c developed by the Federal Republic of Germany (FRG) in a cooperative program with NASA

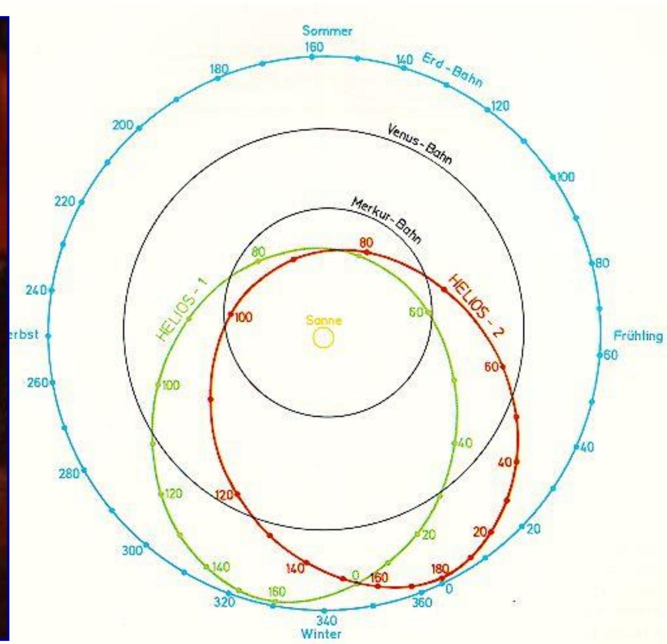

- Two spacecraft, launched in 1974(10 Dec) & 1976(15 Jan)
- ecliptic orbit, perihelium @ 0.29AU
- Plasma measurements: protons(+alphas) and electrons
- Slow plasma sampling, VDF in 40.5 sec
- Low phase space resolution
- NO composition
- NO imaging

Programme realized in only 5 years!

1969: contract between FRG and NASA approved

10 December 1974: Helios 1 launched

Helios instruments

Tabelle 1: Übersicht über die Experimente auf Helios

Nr.	Thema	Experimentatoren	Institut
1	Sonnenwind	H. Rosenbauer, R. Schwenn	MPI für Physik und Astrophysik, Institut für extraterrestrische Physik, Garching
		J. H. Wolfe	NASA Ames Research Center
2/4	Interplanetares	G. Musmann, G. Dehmel, F. M. Neubauer, A. Maier	TU Braunschweig, Institut für Geophysik und Meteorologie
3	Magnetfeld	N. F. Ness, L. F. Burlaga	NASA Goddard Space Flight Center
		F. Mariani	Universität Rom, Istituto di Fisica
5	Elektrische	D. A. Gurnett	Un. of Jowa, Dep. of Physics and Astronomy, Jowa City
	Felder,	P. J. Kellogg	Un. of Minnesota, School of Physics and Astronomy, Minneapolis
	Radiowellen	R. R. Weber	NASA Goddard Space Flight Center
6	Kosmische	H. Kunow, G. Green, R. Müller, G. Wibberenz	Un. Kiel, Institut für Reine und Angewandte Kernphysik
7	Strahlung	J. H. Trainor, K. G. McCracken	NASA Goddard Space Flight Center
		F. B. McDonald	Un. of New Hampshire
		E. C. Roelof, B. J. Teegarden	SCIRO, Melbourne, Australien
8	Strahlung mittlerer Energie	E. Keppler, G. Umlauft, B. Wilken	MPI für Aeronomie, Lindau
		Williams	ESSA, Boulder
9	Zodiakallicht	C. Leinert, H. Link, E. Pitz	MPI für Astronomie, Heidelberg
10	Mikrometeoriten	E. Grün, P. Gammelin, J. Kissel	MPI für Kernphysik, Heidelberg
11	Relativitätstheorie	W. Kundt, O Böhringer	Un. Hamburg, Institut f. Theor. Physik
		W. G. Melbourne, I. D. Anderson	JPL, Pasadena
12	Faraday Rotation	H. Volland, M. Bird	Un. Bonn, Radioastron. Institut
		G. S. Levy	JPL, Pasadena
12 Z	Elektronendichte der Korona	P. Edenhofer, E. Lüneburg	DFVLR Oberpfaffenhofen

Plasma Experiment 1.

Magnetic Field Experiments 2. 3. 4.

Plasma Wave Experiment 5.

Cosmic Radiation Experiment 6. 7.

Low-Energy Electron and Ion Spectrometer 8.

Zodiacal Light Photometer 9.

Micrometeorid Analyser 10.

Helios lifetime during solar cycles 20 - 21

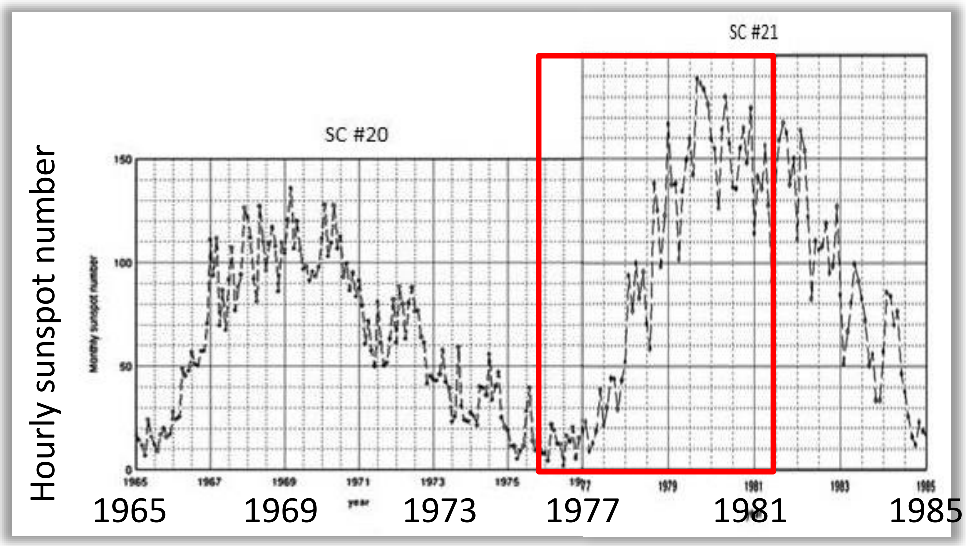

Best data coverage during primary missions to the Sun during 1975 and 1976

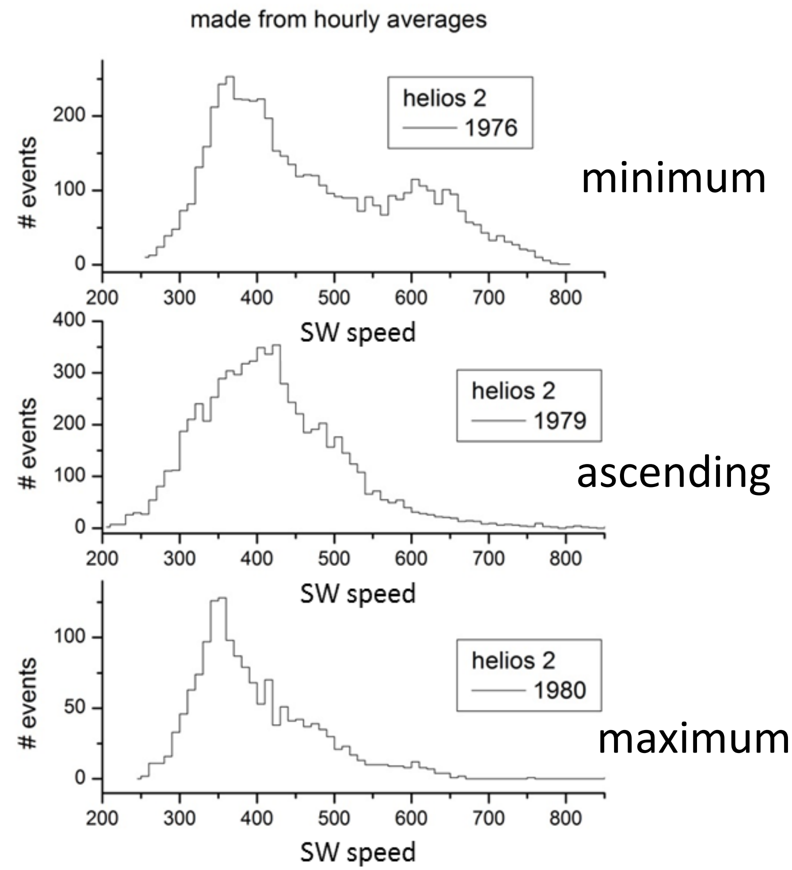

Bimodal nature of solar wind particularly clear during solar minimum

First Helios observations

Decreasing distance

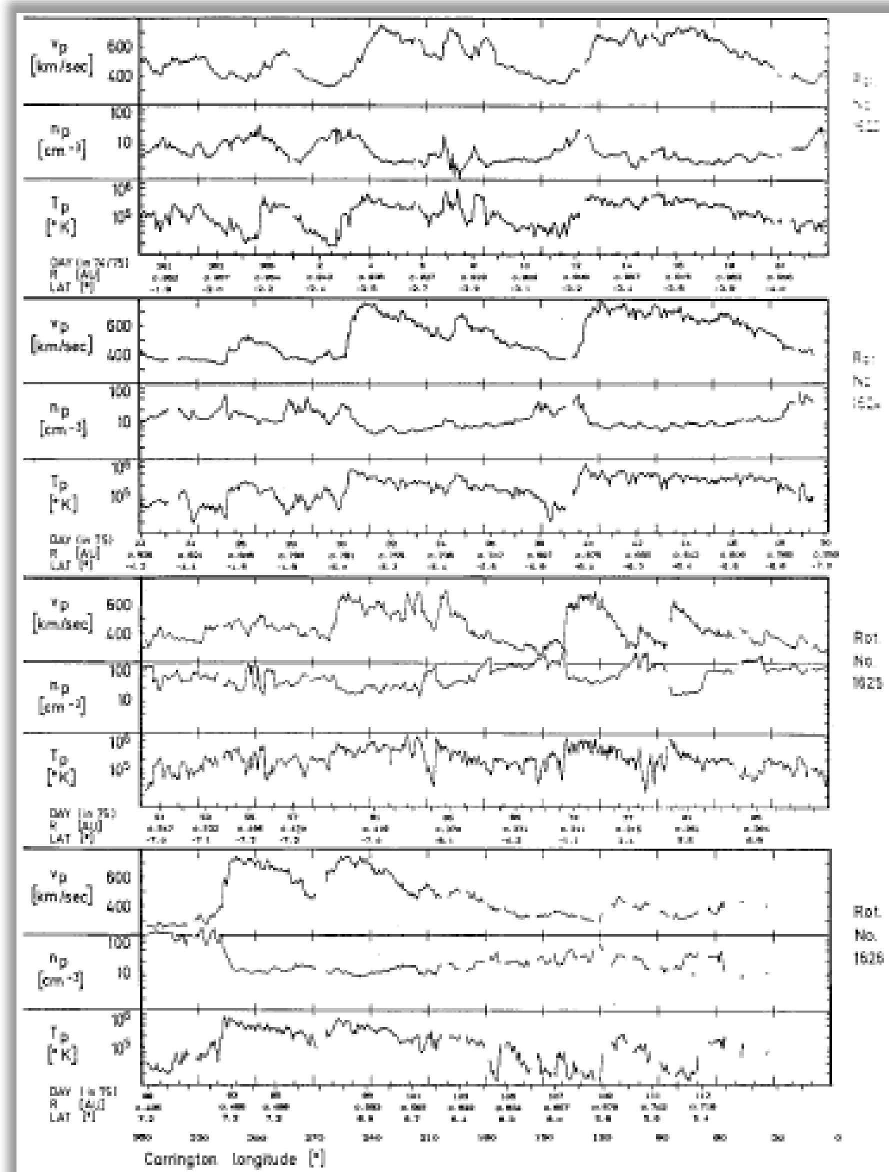

@ 1 AU

- Broad high-speed streams with v_p ~ 700 km/s, n_p ~ 3 cm^{-3}, T_p ~ $2{\cdot}10^5$ K

- Regions of slow solar wind with v_p ~ 400 km/s, n_p ~ 10 cm^{-3} and T_p ~ $4{\cdot}10^4$ K, highly variable

With decreasing distance, we observe a steepening of the fast streams' leading edges

(Schwenn, 1990)

First detailed studies on the dynamical interaction between fast and slow wind

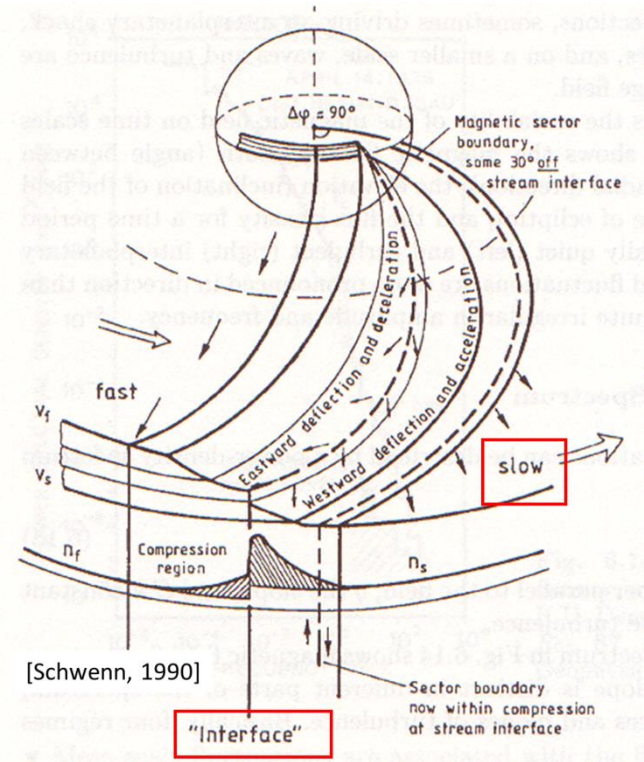

Dynamical interaction steepens the speed profile

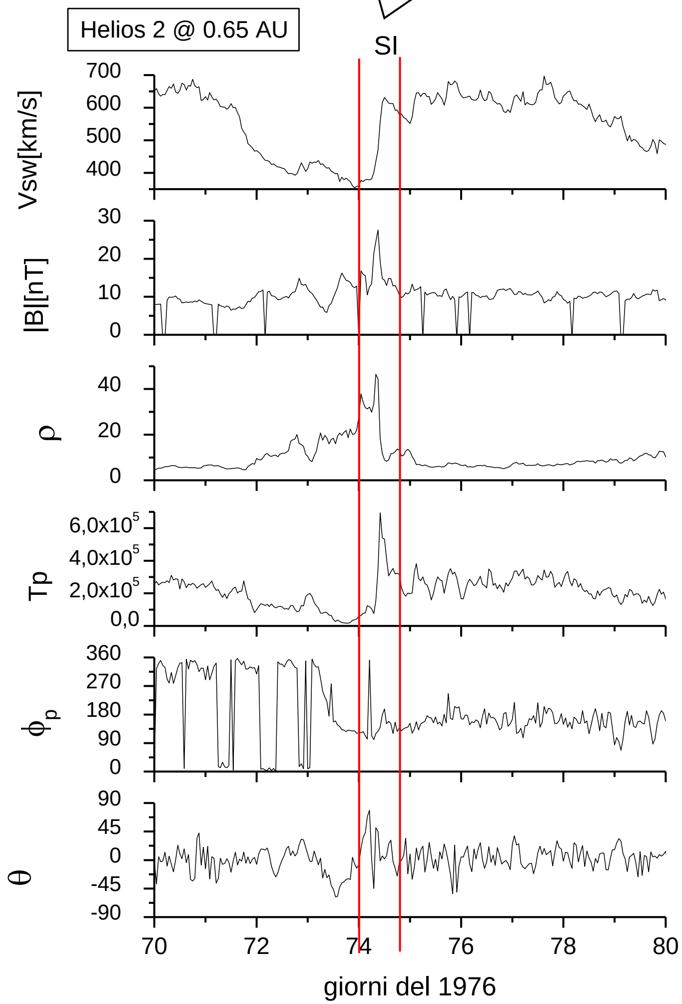

- The interactions of slow and fast solar wind at the leading edges of high speed streams causes compression to high plasma densities and deflections of the flow on both sides: westward in the slow plasma and estward in the fast plasma

Fast wind interacts with the slow wind ahead creating a compression region called *stream-interface*

Macrostructure of the interplanetary magnetic field

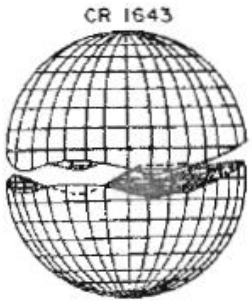

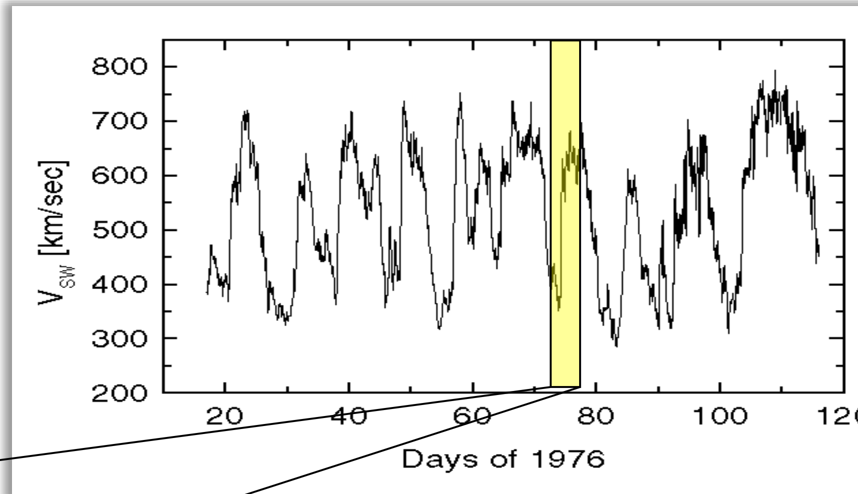

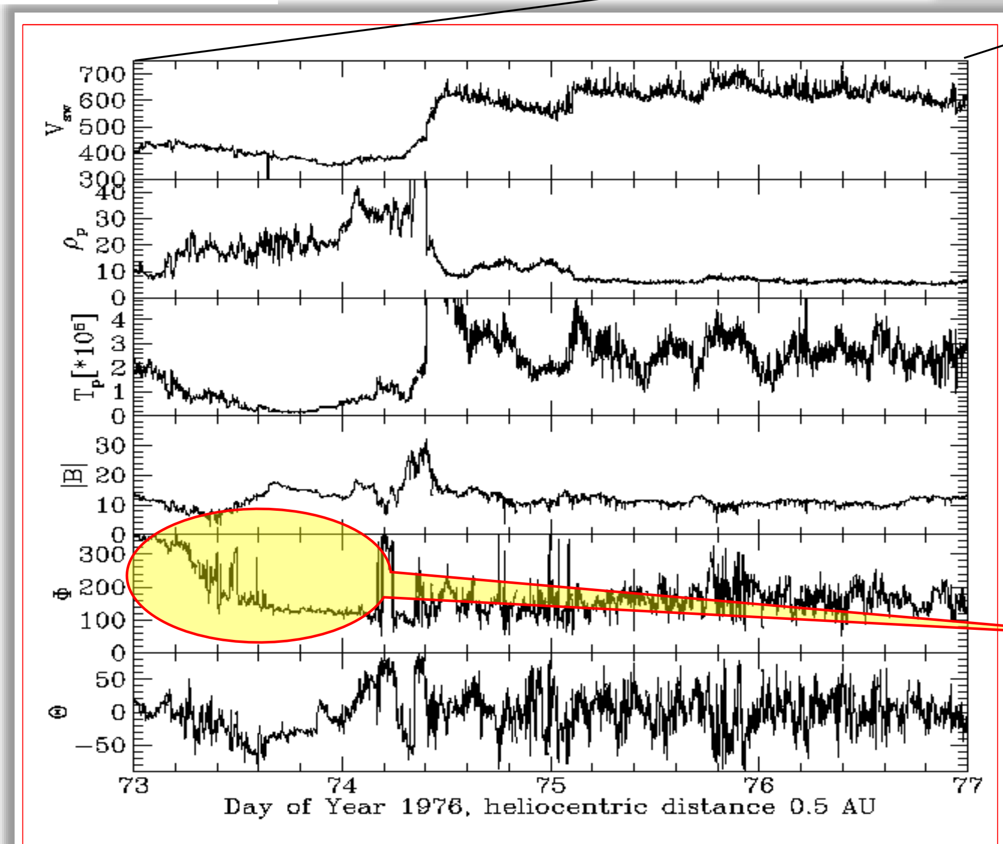

Helios crossed the Heliospheric Current Sheet several times along its orbit.

The Ballerina model
[Schulz-Levy-Alfvén model (1973-1977)]

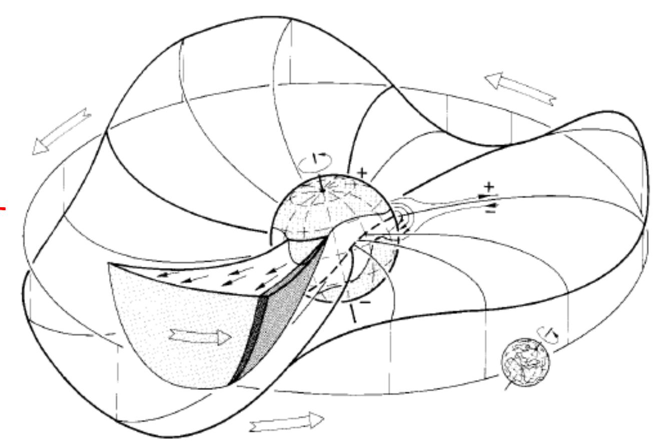

The crossing of the HCS at short heliocentric distances

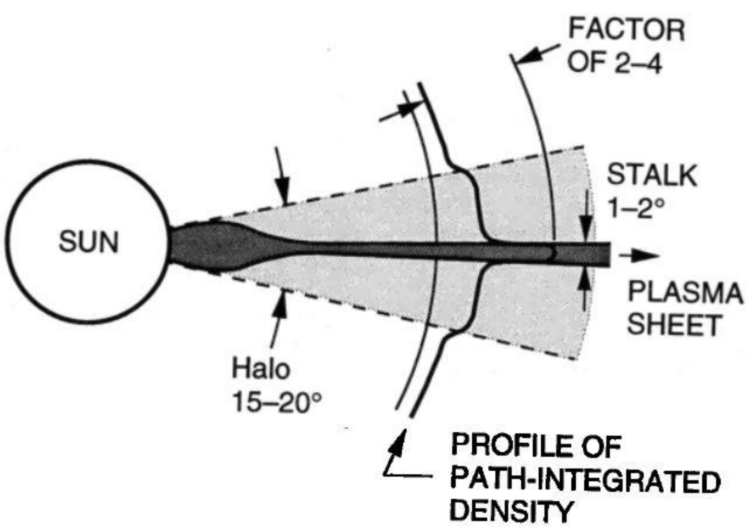

Figure 5. An idealized coronal streamer and its stalk, which forms the plasma sheet in interplanetary space. The radial extension of the boundaries of the streamer are responsible for the observed density halo. The profile of path-integrated density is also shown.

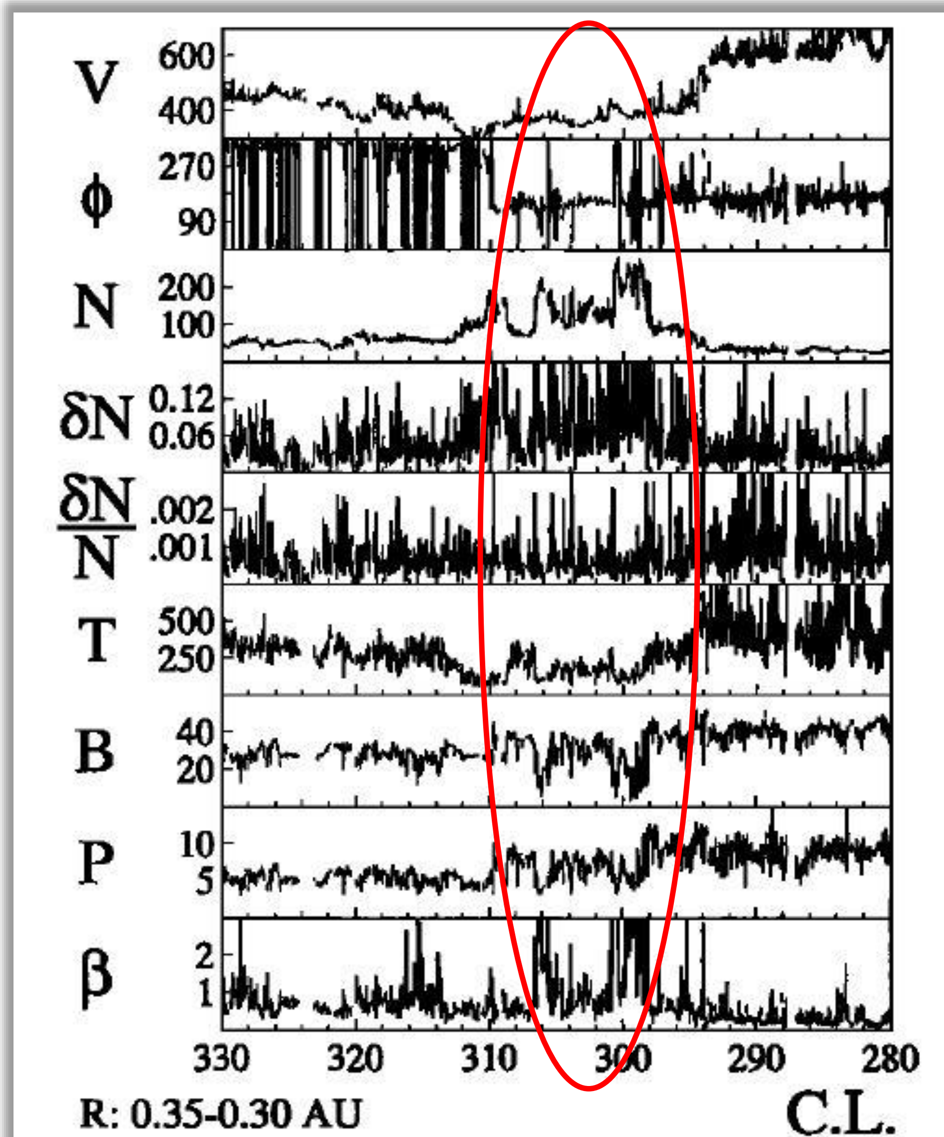

[Bavassano et al., 1997]

Importance of separating fast from slow wind

- Fast and slow wind features should never be averaged together.

«Asking for the average solar wind might appear as silly as asking for the taste af an average drink. What is the average between wine and beer? Obviously a mere mixing – and averaging means mixing – does not lead to a meaningful result.
Better taste and judge separately and then compare, if you wish.»

[Rainer Schwenn, Solar Wind 5, 1982]

Differences in the Alfvénic character of the fluctuations

$$v_{az} = sign[-\vec{k} \cdot \vec{B}_0] \frac{b_z}{\sqrt{4\pi\rho}}$$

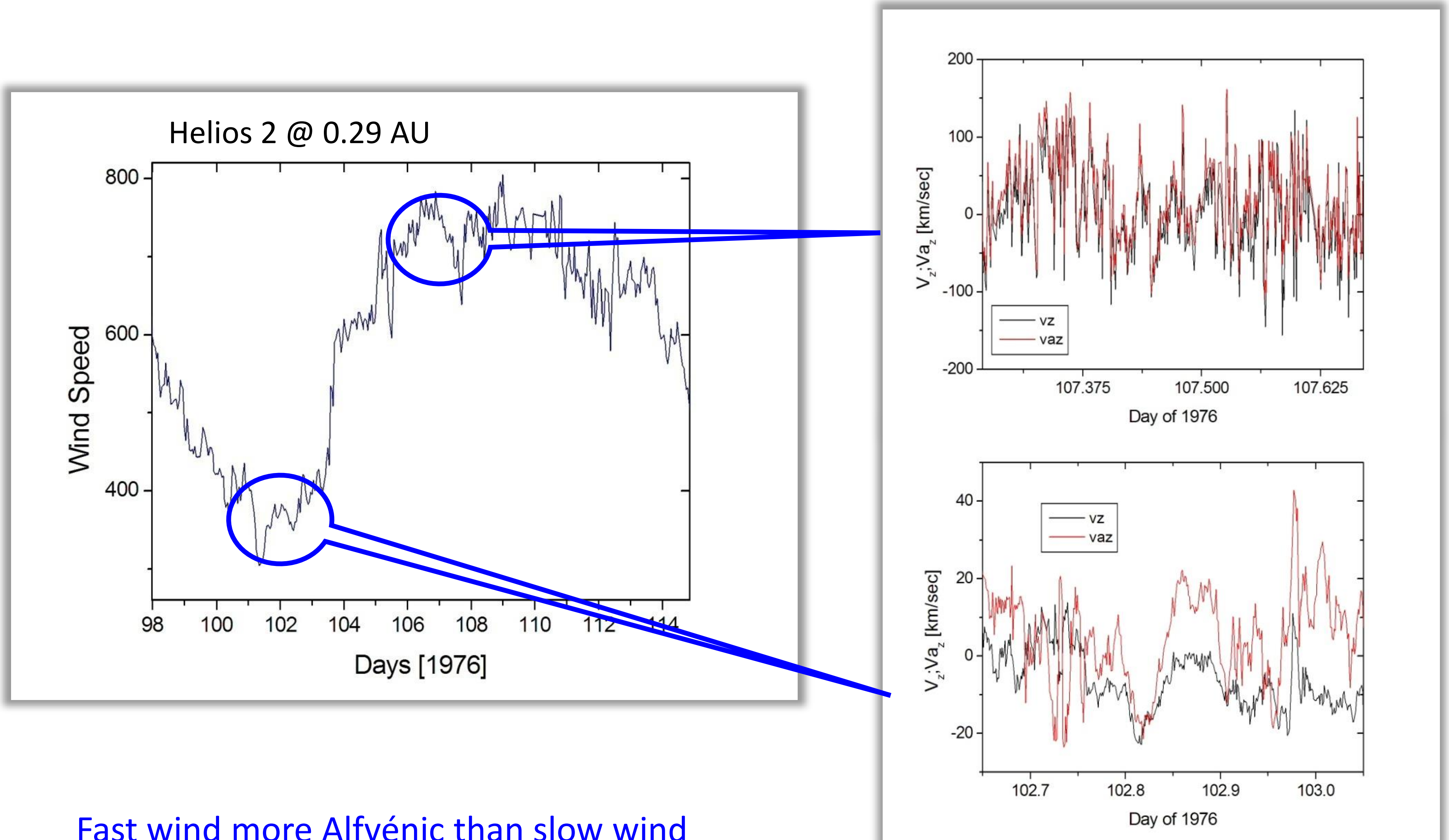

Fast wind more Alfvénic than slow wind

Differences in the δB-δV alignment

$$\hat{\theta}_\tau = \cos^{-1}\left\langle \frac{\Delta\vec{v}_\tau(t)\cdot\Delta\vec{b}_\tau(t)}{|\Delta\vec{v}_\tau(t)||\Delta\vec{b}_\tau(t)|}\right\rangle_t$$

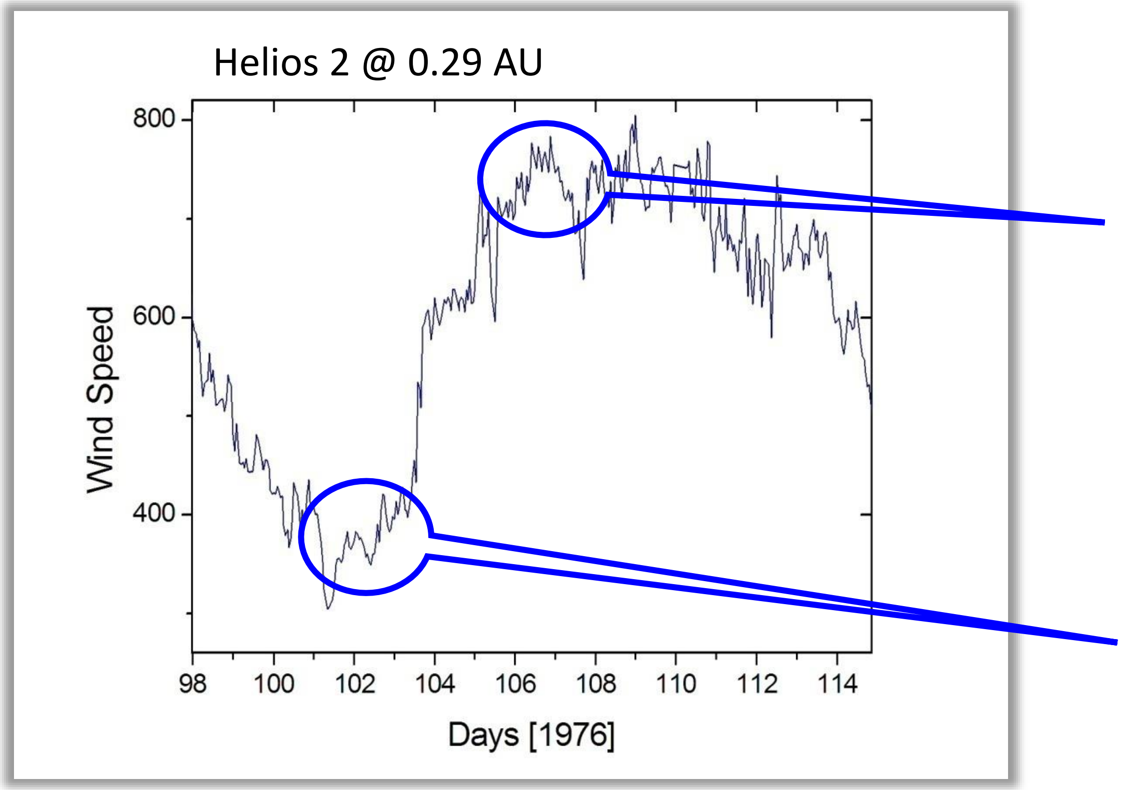

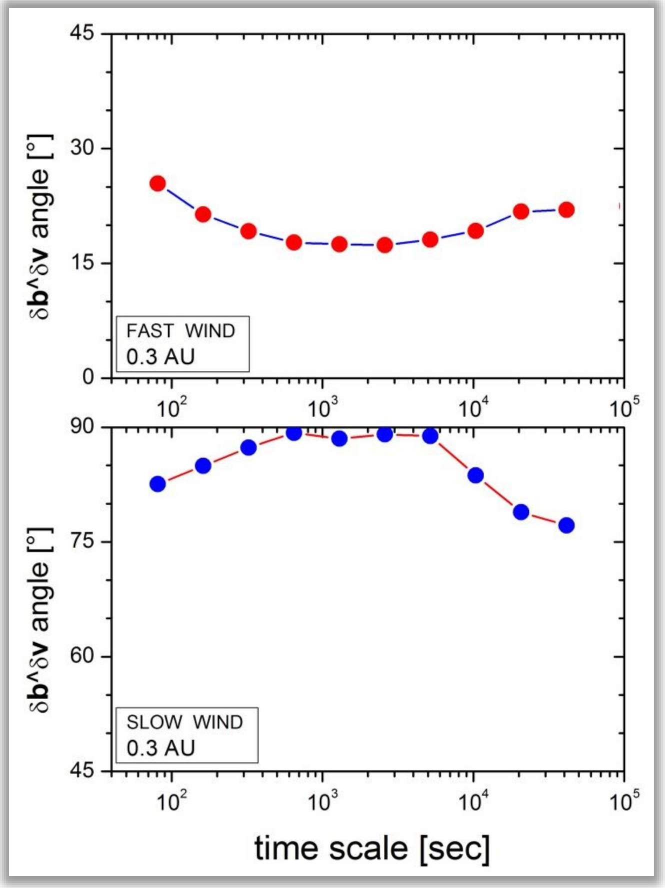

$\vec{b}$ and $\vec{v}$ quite aligned within fast wind
best alignment ~ 20-30 min

Differences in the spectral signature

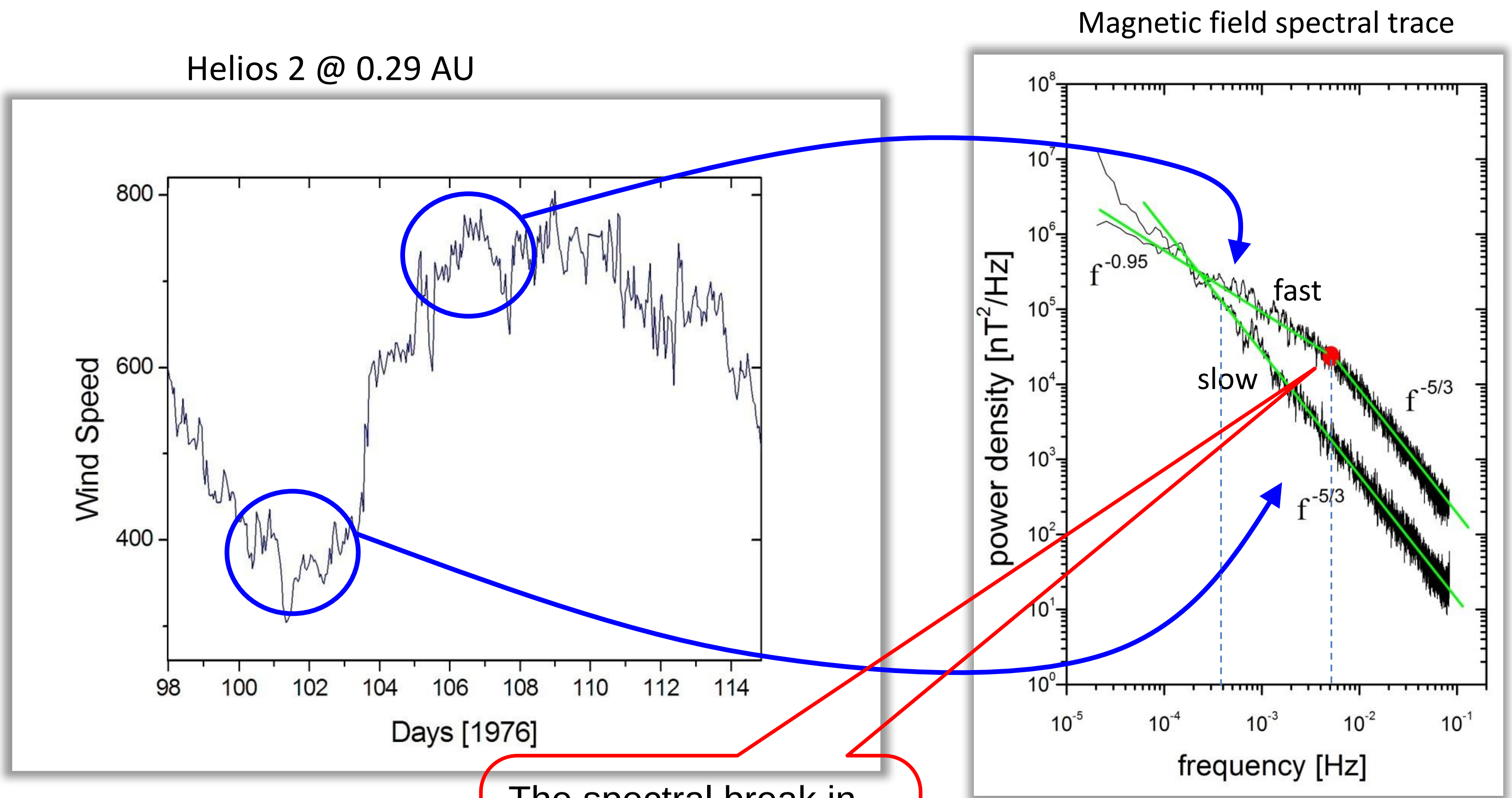

The spectral break in the fast wind spectrum suggests shorter correlation lengths

Differences in the correlation length

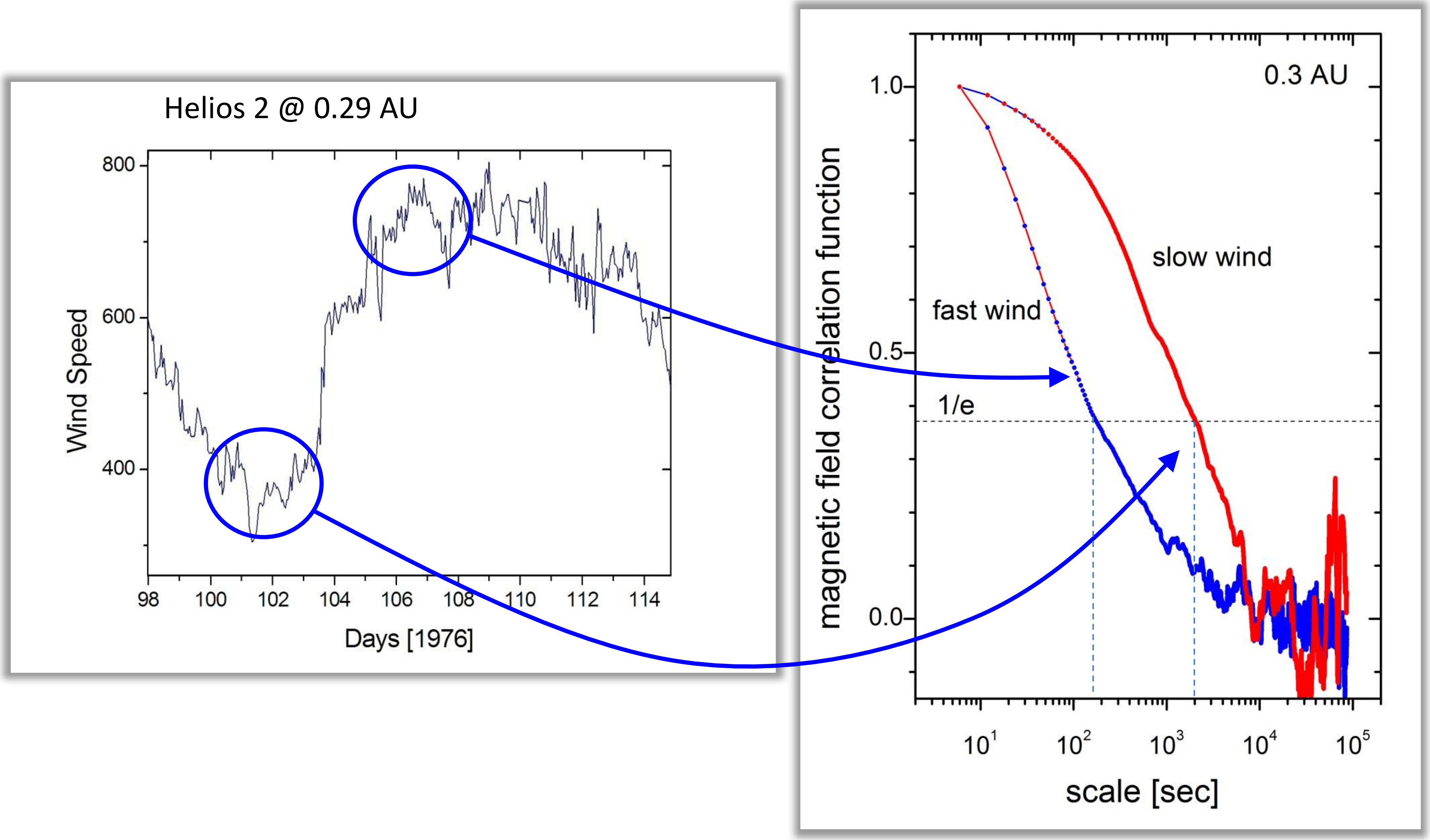

The solar wind power spectrum is characterized by a power-law whose spectral slope is "universal"

IMF power spectrum at 1 AU
(Low freq. from *Bruno el al*, 1985; high freq. Tail from *Leamon et al*, 1999)

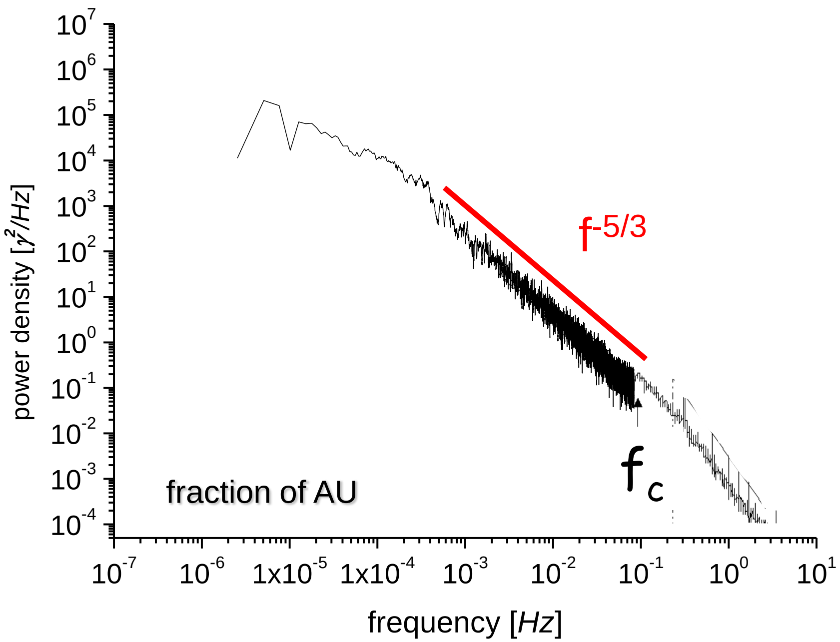

Laboratory experiment with low temperature helium gas flow

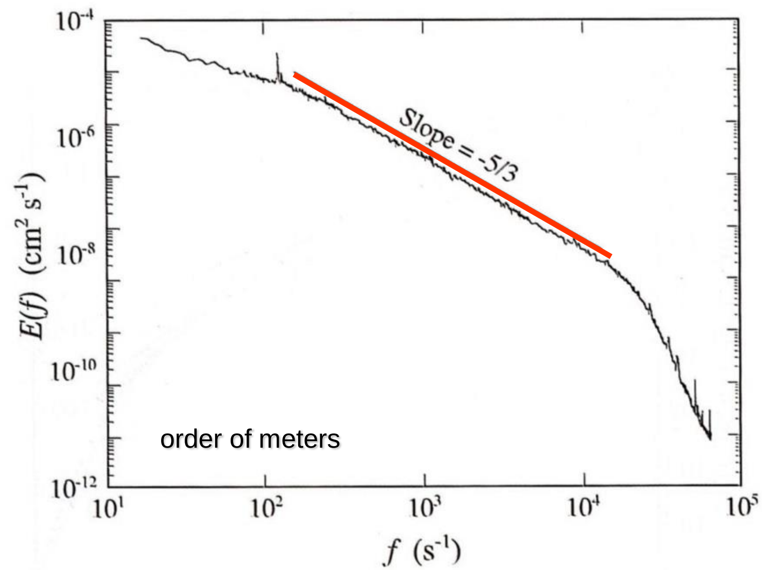

(*Maurer et al*., 1994)

The spectrum of turbulence is characterized by a power-law whose spectral slope is "universal"

IMF power spectrum at 1 AU
(Low freq. from *Bruno el al*, 1985; high freq. Tail from *Leamon et al*, 1999)

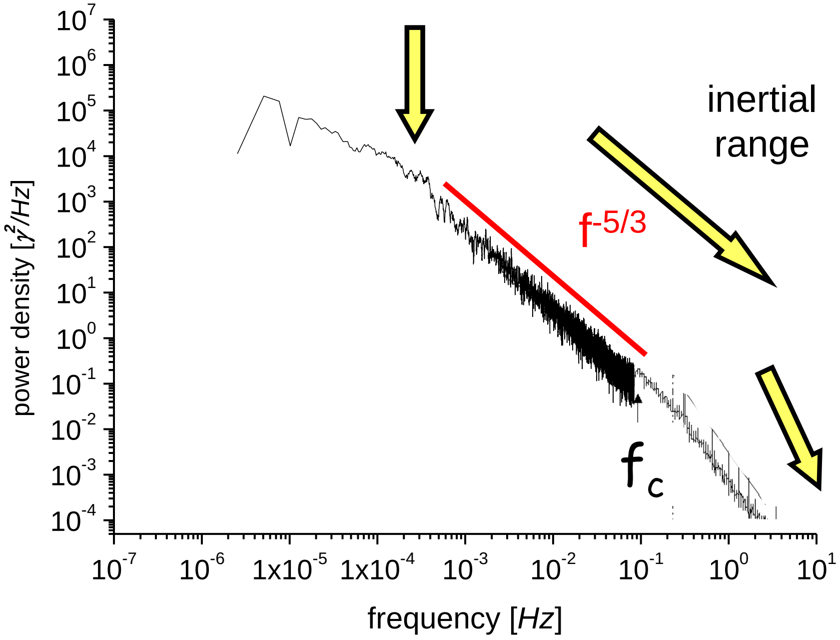

Cascade *à la Richardson*

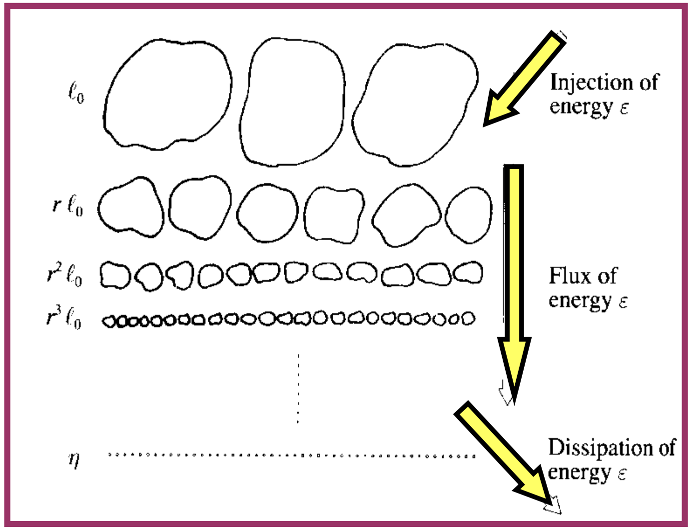

(*Frisch*, 1995)

Navier-Stokes equations

fluid

$$\frac{\partial \vec{v}}{\partial t} + \left(\vec{v} \cdot \nabla\right)\vec{v} = -\nabla P + \nu \nabla^2 \vec{v}$$

Non-linear term

Dissipative term

MHD

$$\frac{\partial \vec{z}^{\pm}}{\partial t} + \left(\vec{z}^{\mp} \cdot \nabla\right)\vec{z}^{\pm} = -\nabla P + \frac{\nu + \mu}{2} \nabla^2 \vec{z}^{\pm}$$

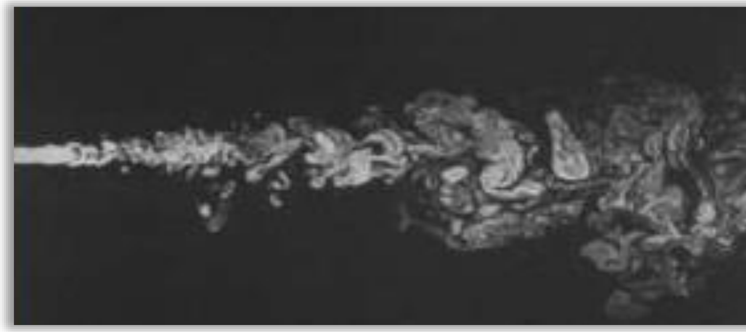

Reynolds number

$$R = \frac{nonlinear}{dissipative} \approx 10^5$$

(*Matthaeus et al*, 2005)

Nonlinear interactions and the consequent energy cascade need both Z^+ and Z^- to be present at the same time

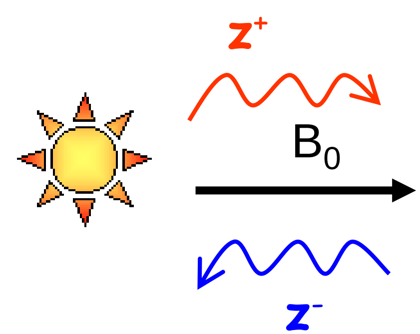

$$\vec{z}^{\pm} = \vec{v} \pm \vec{b} = \vec{v} \pm \vec{B} / \sqrt{4\pi\rho}$$

Elsässer variables

Differences in the power associated to e⁺ and e⁻

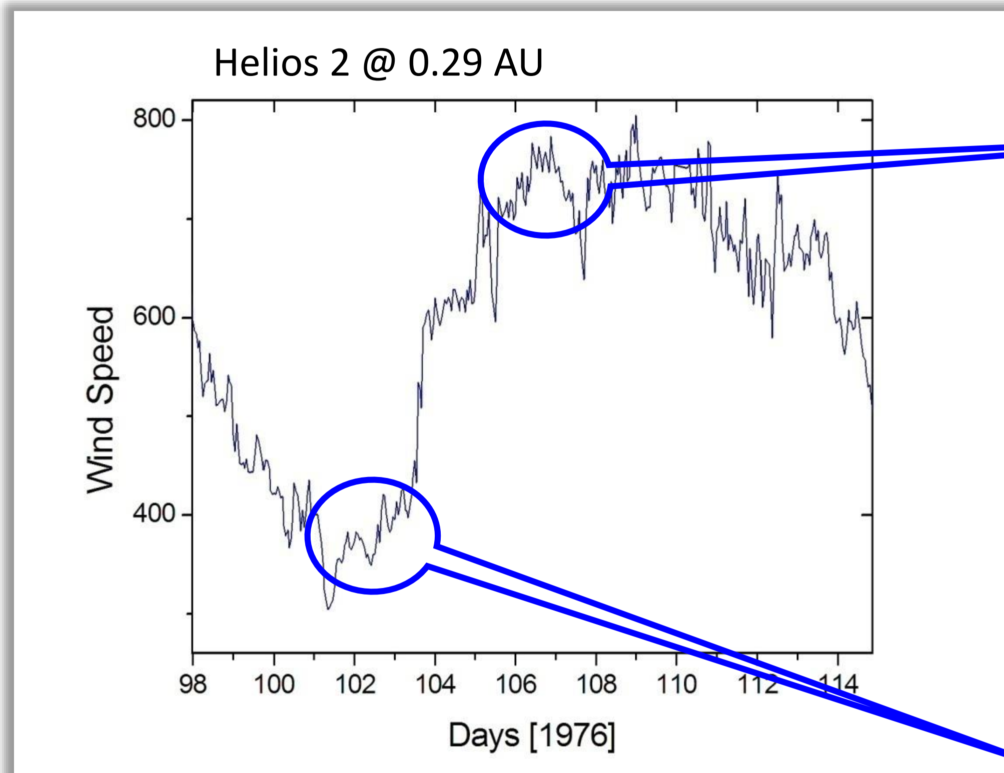

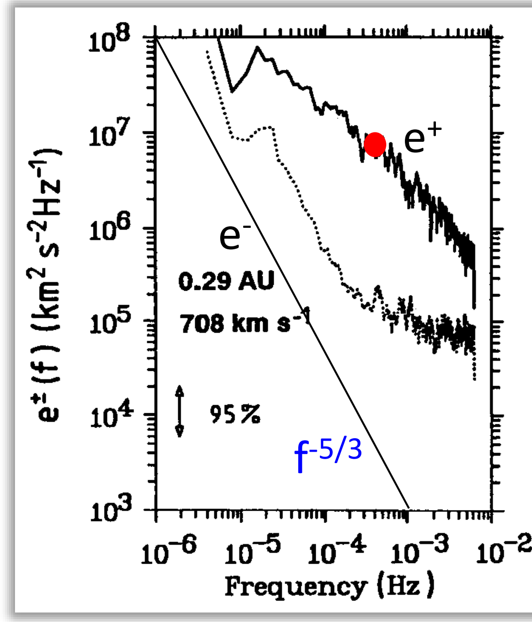

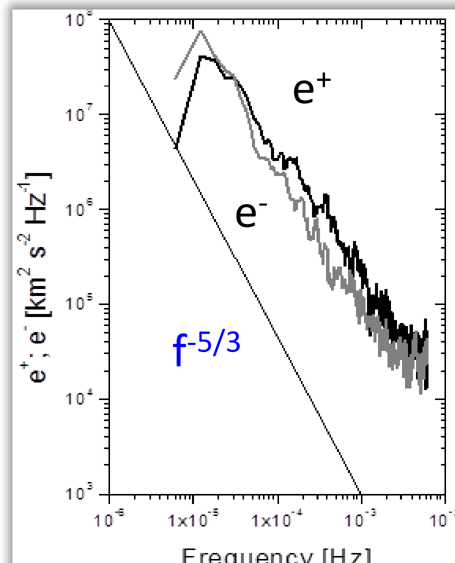

[Tu et al., 1990]

Fast wind: e^+ is much higher than e^-
e⁺: break; a flatter slope at low frequencies; a Kolmogorov-like slope at higher frequencies.
e^- : break; Kolmogorov slope at low frequencies; a sort of plateau at higher frequencies.

Slow wind: both spectra have almost equivalent power density and follow the Kolmogorov slope.

Differences in the level of normalized crosshelicity

$$\sigma_c(f) = \frac{e^+(f) - e^-(f)}{e^+(f) + e^-(f)}$$

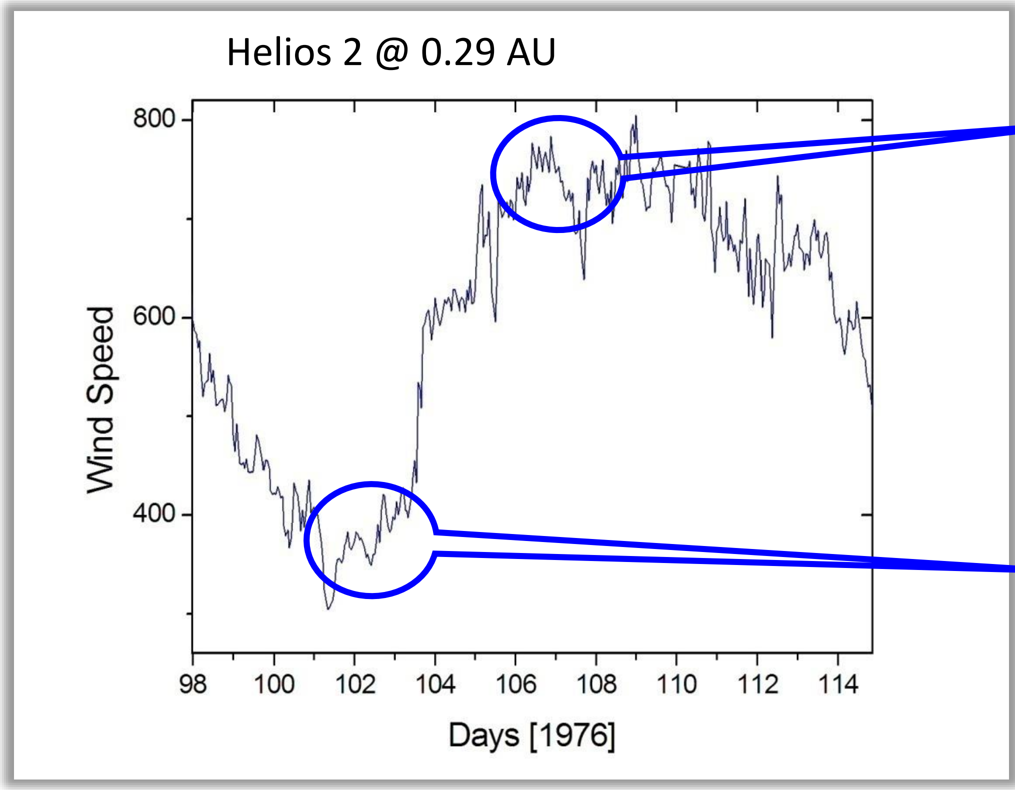

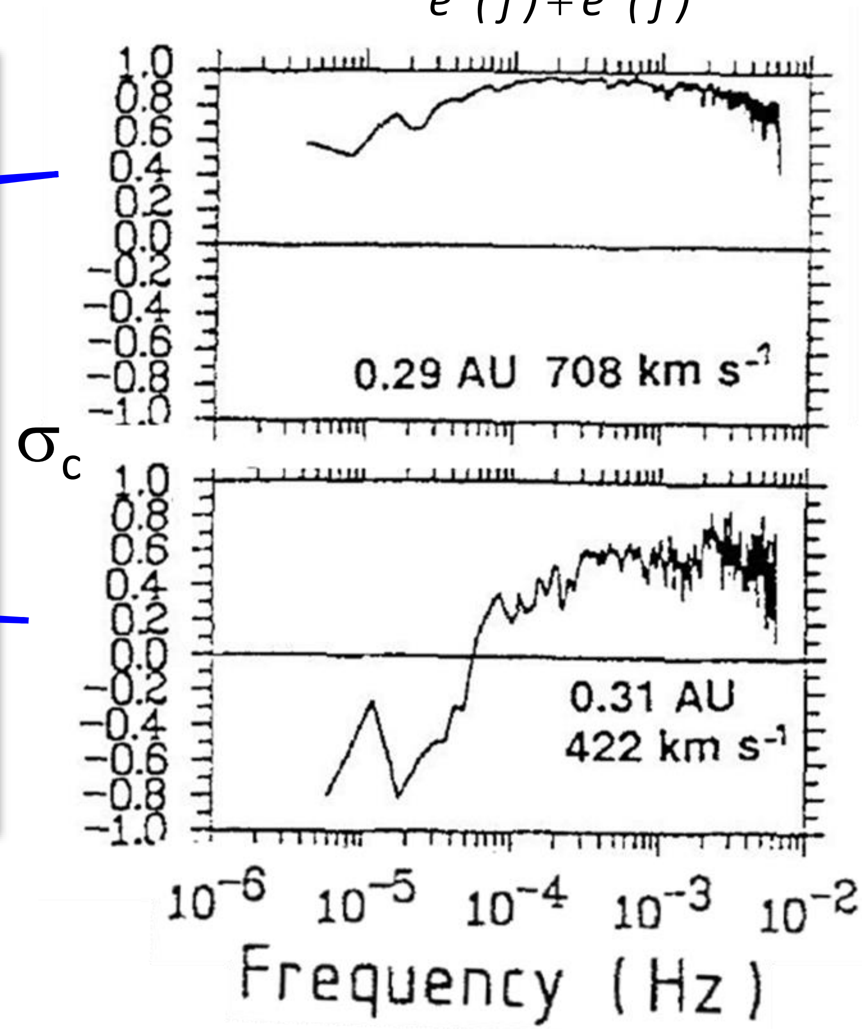

Higher values in fast wind

[adapted from Marsch and Tu, 1990]

Differences in the level of magnetic and kinetic energy content

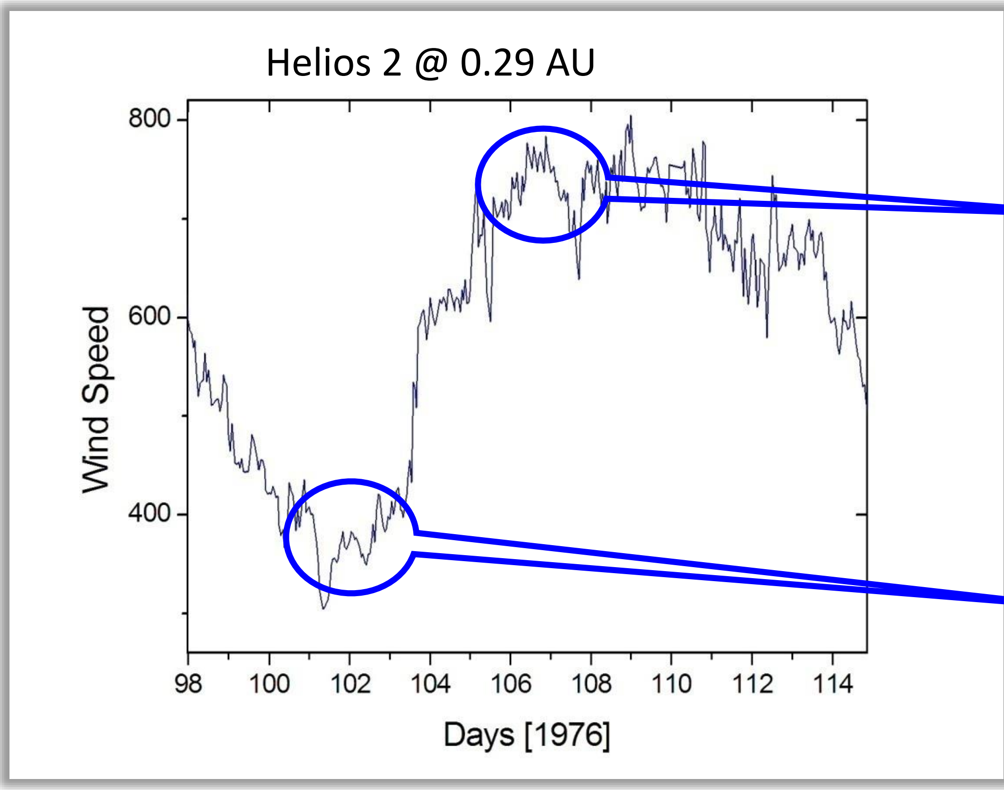

Close to equipartition

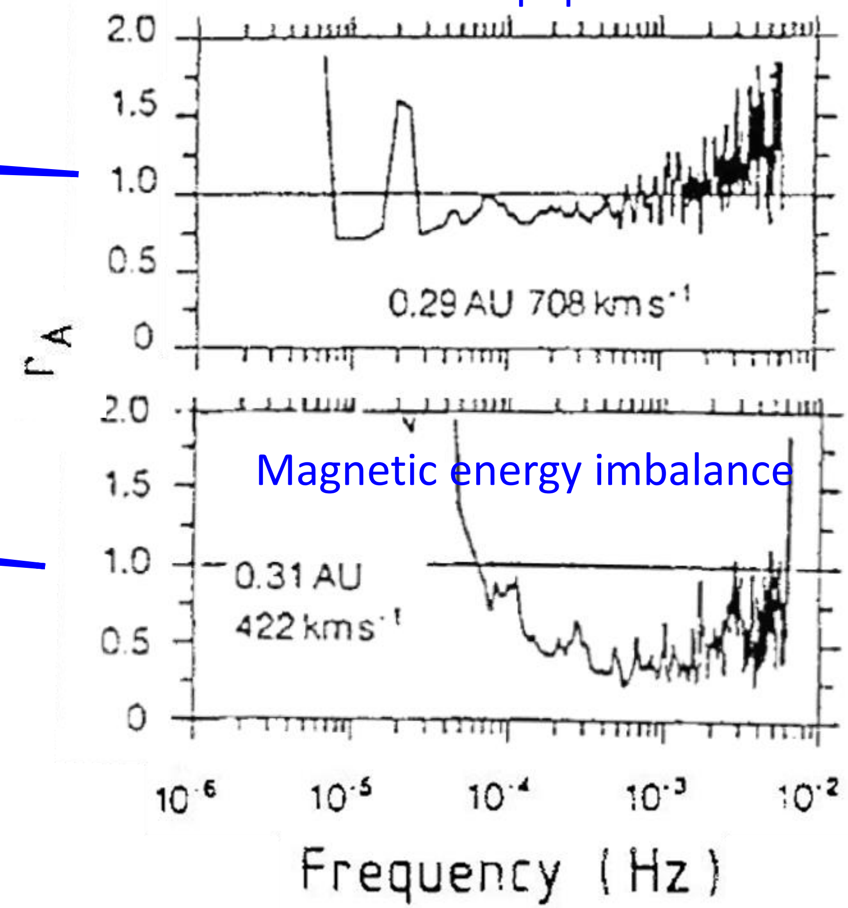

$$r_A(f) = \frac{e_v(f)}{e_b(f)}$$ Alfvén ratio

[adapted from Marsch and Tu, 1990]

Power law spectra → scale invariance → self-similarity

A typical IMF power spectrum in interplanetary space at 1 AU [Low frequency from *Bruno et al*., 1985; high freq. tail from *Leamon et al*, 1999]

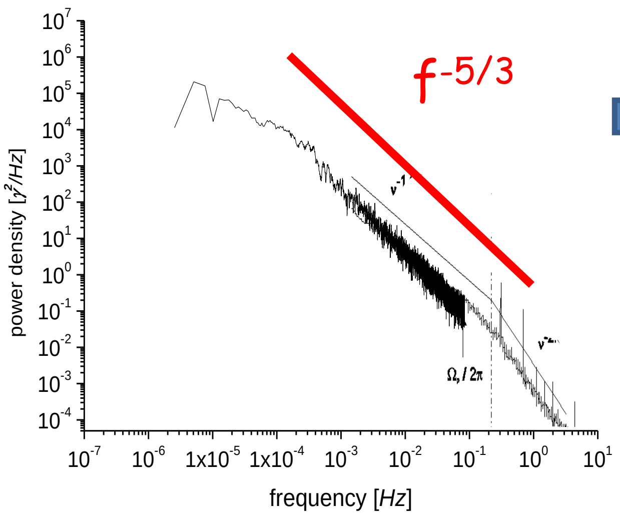

Power law brings scale invariance

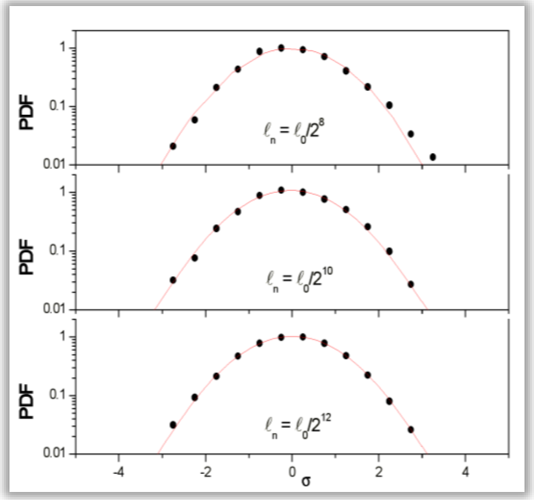

From small to large scales

(numerical simulations)

Scale invariance implies self-similar PDFs

What is intermittency?

Data show that solar wind *PDFs* <u>DO NOT RESCALE</u>

❖ Large scales → Gaussian PDF

❖ Small scales → peaked PDF fatter tail, extreme events more probable

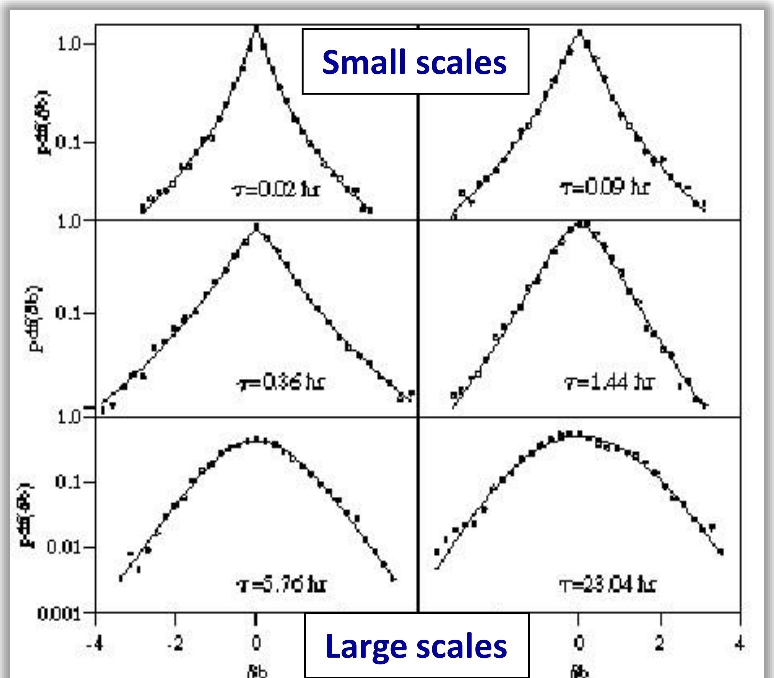

PDFs of magnetic field fluctuations

(Sorriso-Valvo et al., 1999)

The evolution of the shape of the PDF can be measured by the *Flatness* F_τ (fourth order moment) of the distribution itself. An estimate of this parameter can be obtained directly from the structure functions:

$S^p_t = <(x(t+t)-x(t))^p>$

$$F(\tau) = \frac{< S_\tau^4 >}{< S_\tau^2 >^2}$$

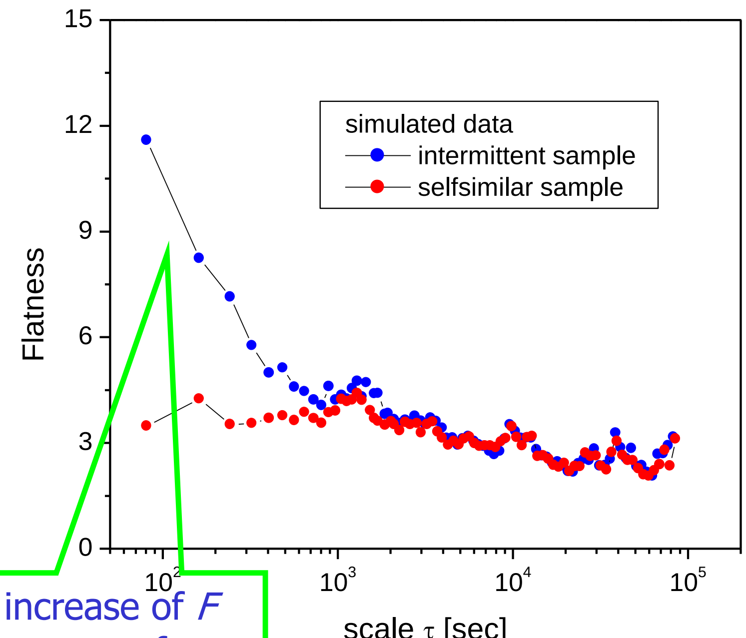

a continuous increase of *F* reveals the presence of intermittency [Frisch, "95].

Different Flatness

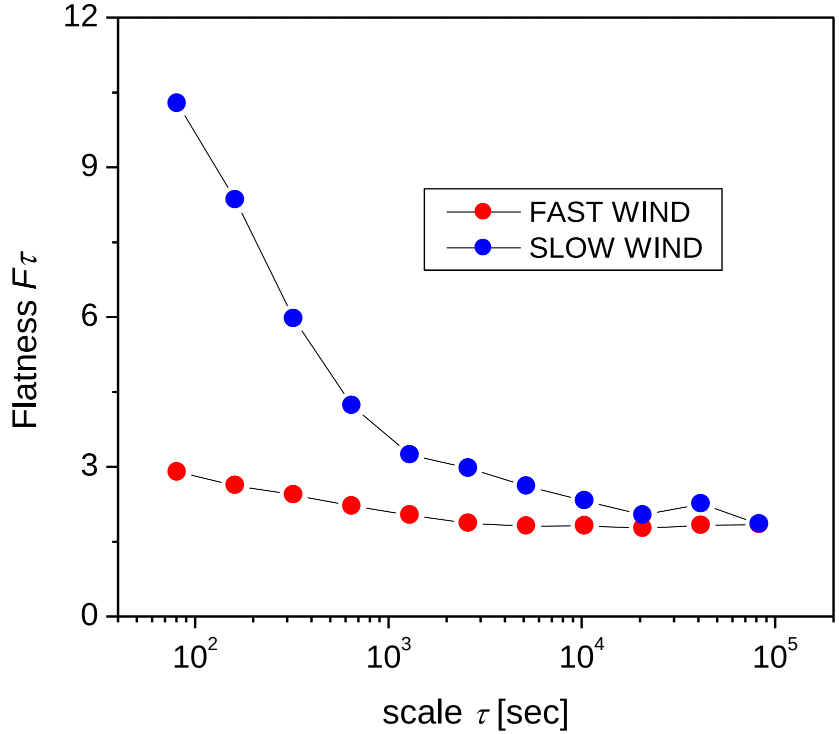

Slow wind:
fluctuations due to convected structures

intermittency

Fast wind:
fluctuations mainly due to stochastic Alfvénic fluctuations

Selfsimilarity
$\Rightarrow$ no intermittency

Radial dependences with Helios

All these features evolve with the radial distance from the Sun in the fast wind

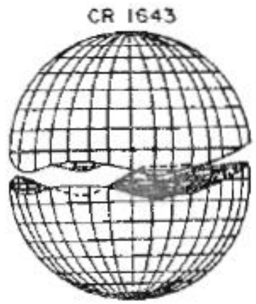

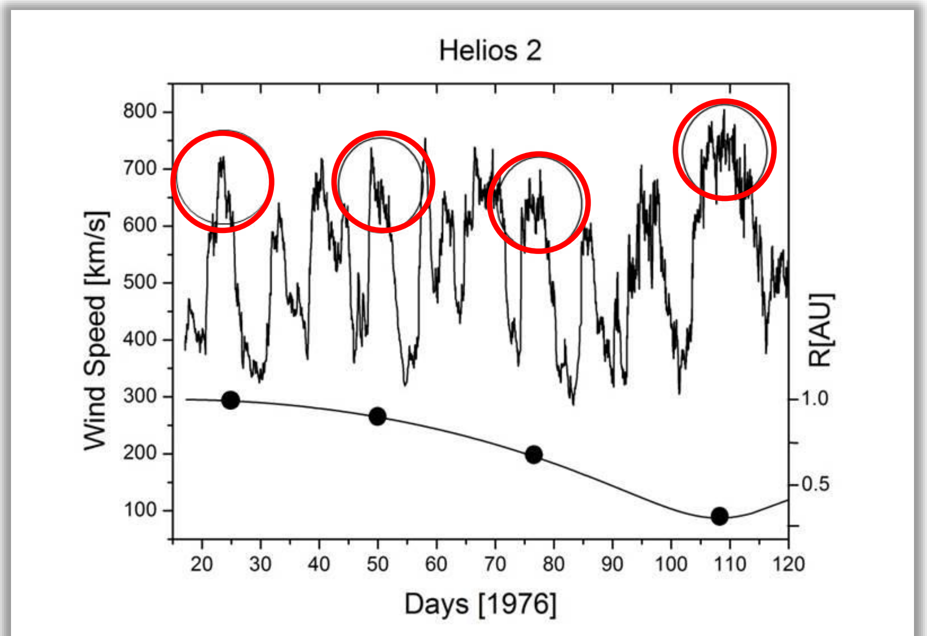

Coronal conditions particularly steady at the Sun allowed to observe the '*same*' corotating stream at different heliocentric distances [Villante (1980) and Bavassano *et al.* (1982)]

Unique chance to study the radial evolution of fluctuations while looking at plasma coming from the same solar source

Evolution of the Alfvénic content

$$\delta\vec{V} = \pm \frac{\delta\vec{B}}{\sqrt{4\pi\rho}}$$

$$\mathrm{sign}[-\vec{k}\cdot\vec{B}_0]$$

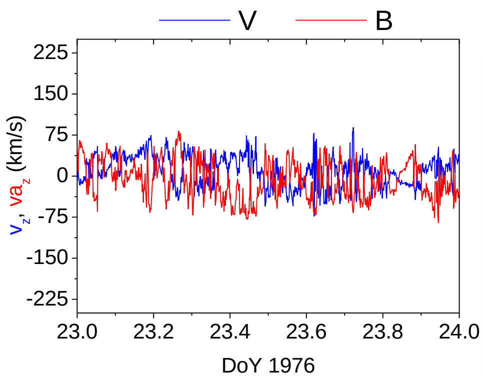

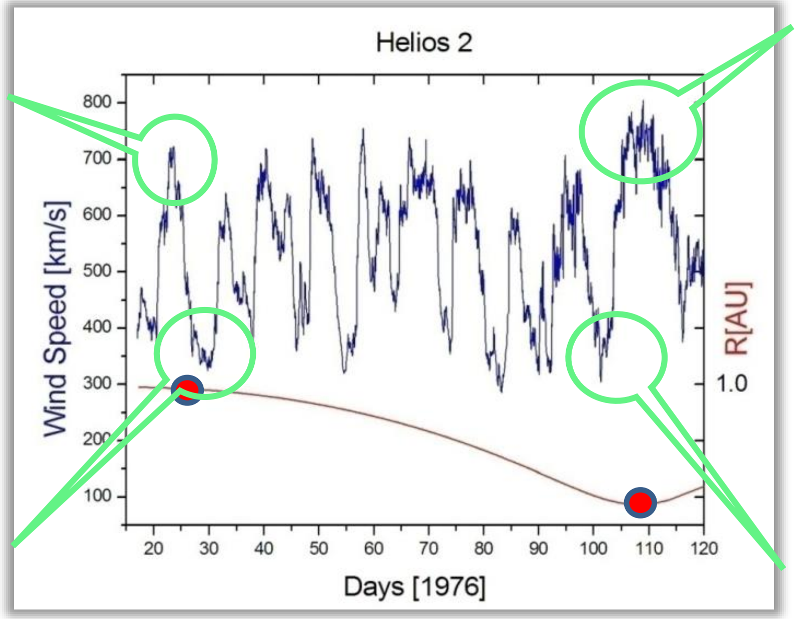

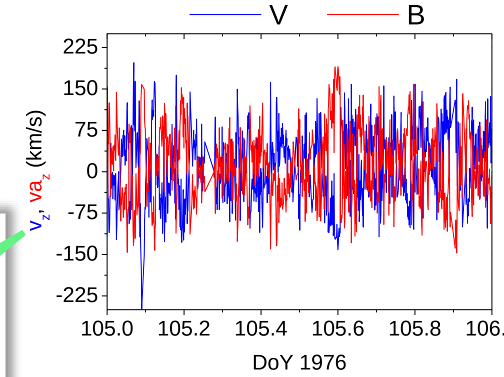

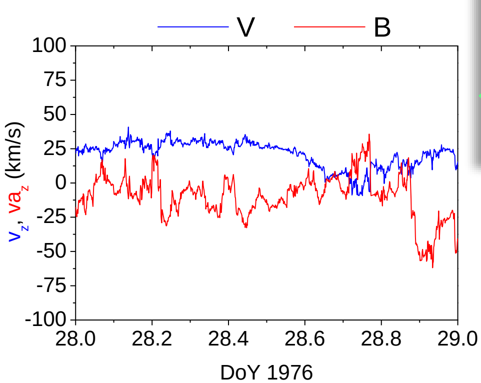

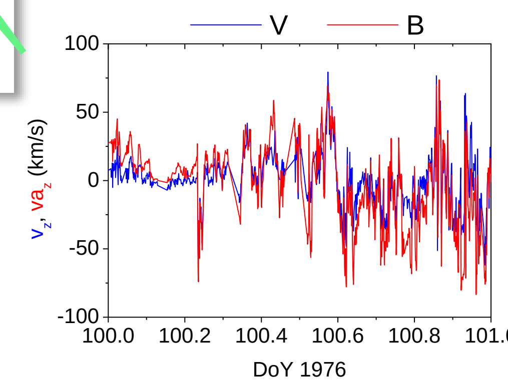

Radial evolution of solar wind turbulence

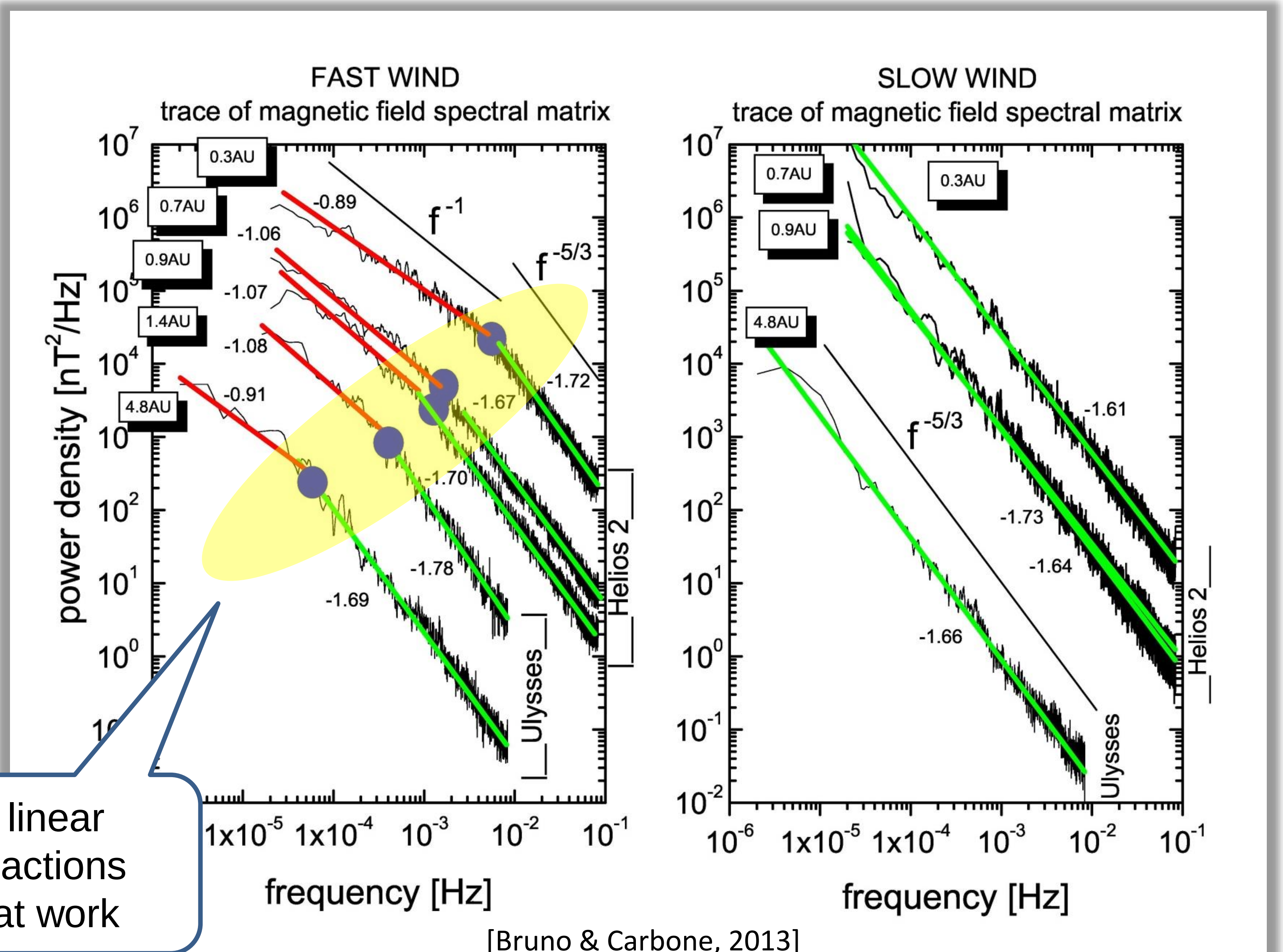

Non linear interactions are at work

[Bruno & Carbone, 2013]

Evolution in the power associated to e^+ and e^-

FAST

For increasing distance:

- e^+ decreases towards e^-
- spectral slope evolves towards -5/3

SLOW

- No much radial evolution
- spectral slopes always close to -5/3

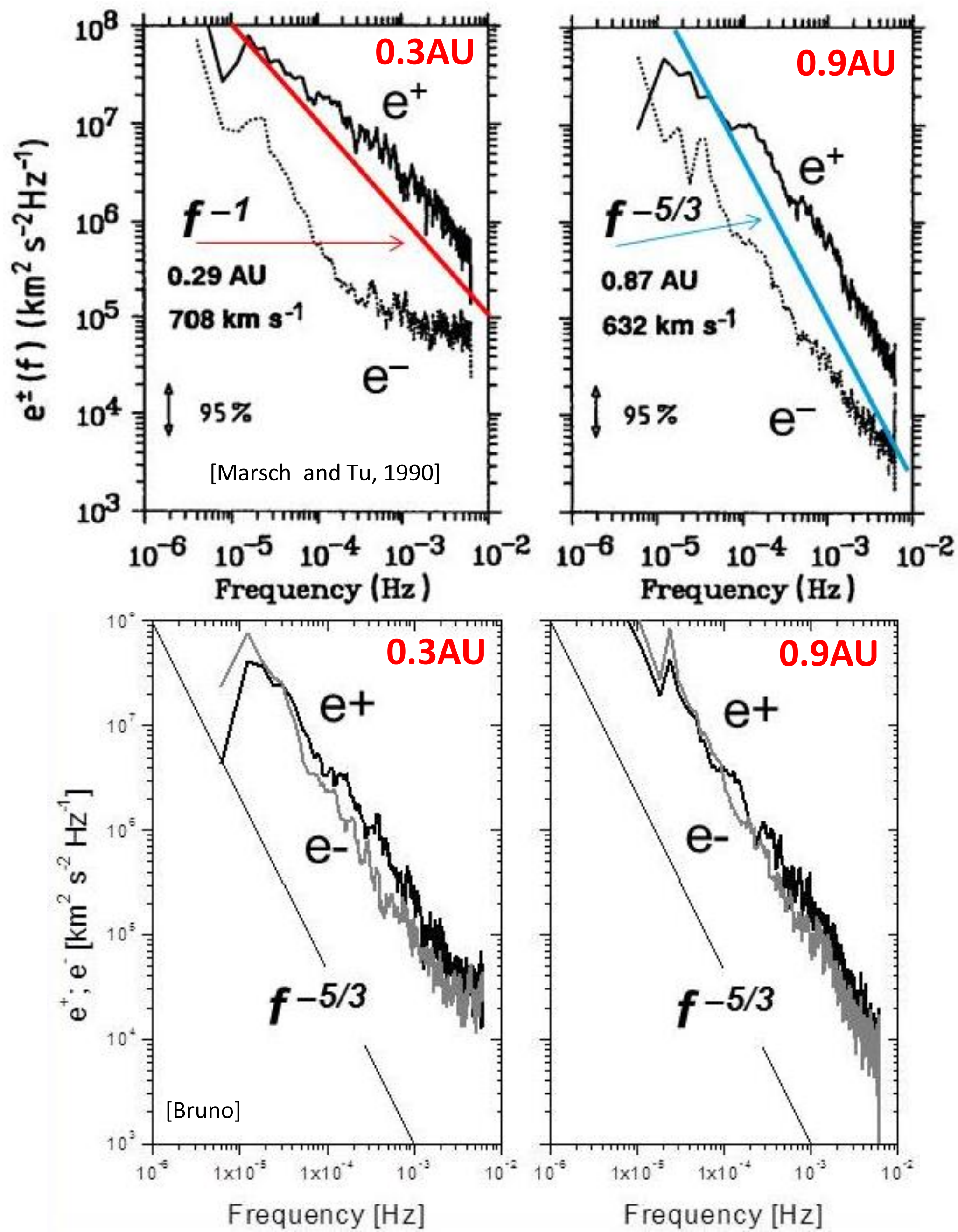

Evolution of δB-δV alignment

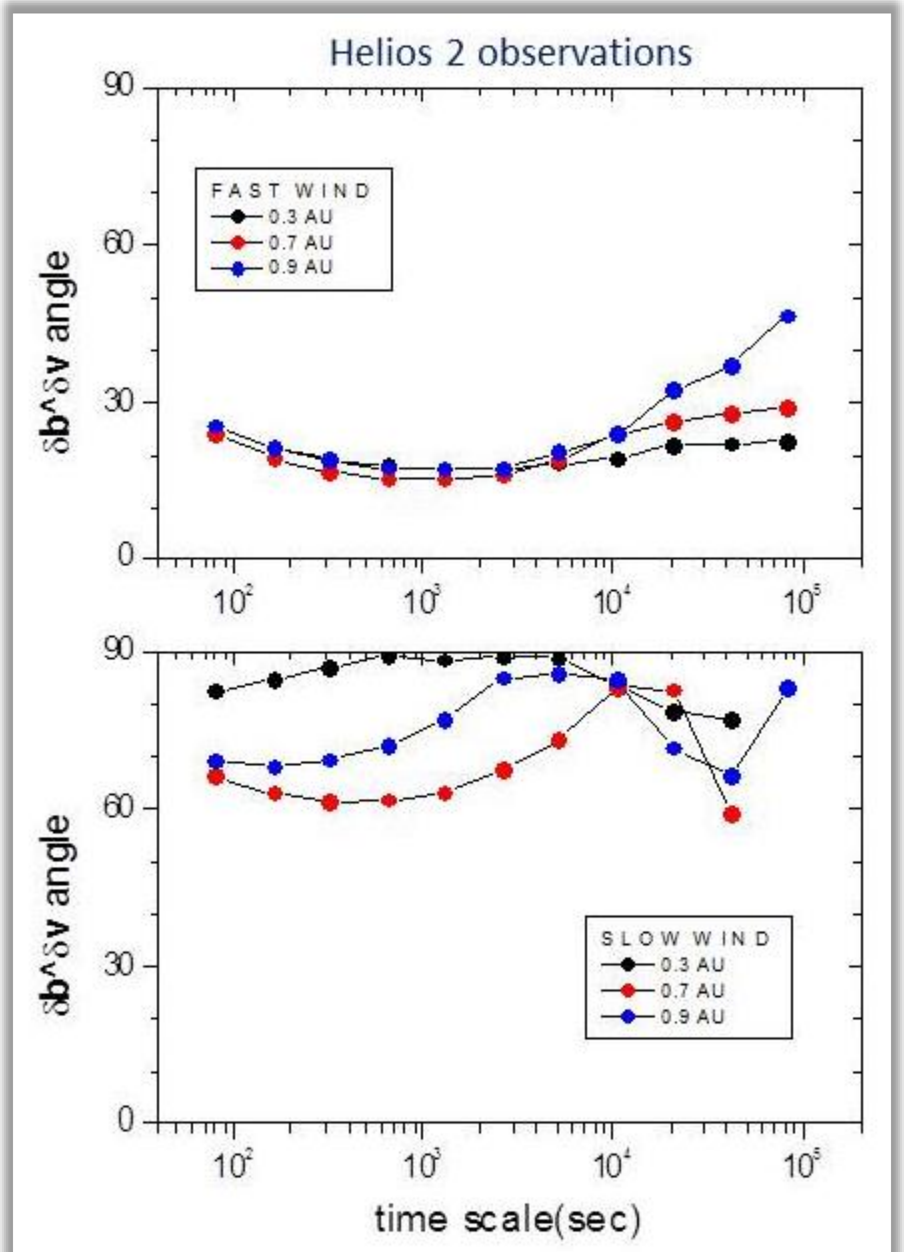

FAST

- Since $e^+ \rightarrow e^-$, $\delta\underline{B}$-$\delta\underline{V}$ alignment decreases during expansion
- Best alignment for younger turbulence (0.3AU)

SLOW

- No alignment for slow wind, as expected from fully developed turbulence ($|\delta Z^+|=|\delta Z^-|$)

Evolution of intermittency

flatness factor F_τ as a function of scale and radial distance from the sun computed for magnetic field vector fluctuations

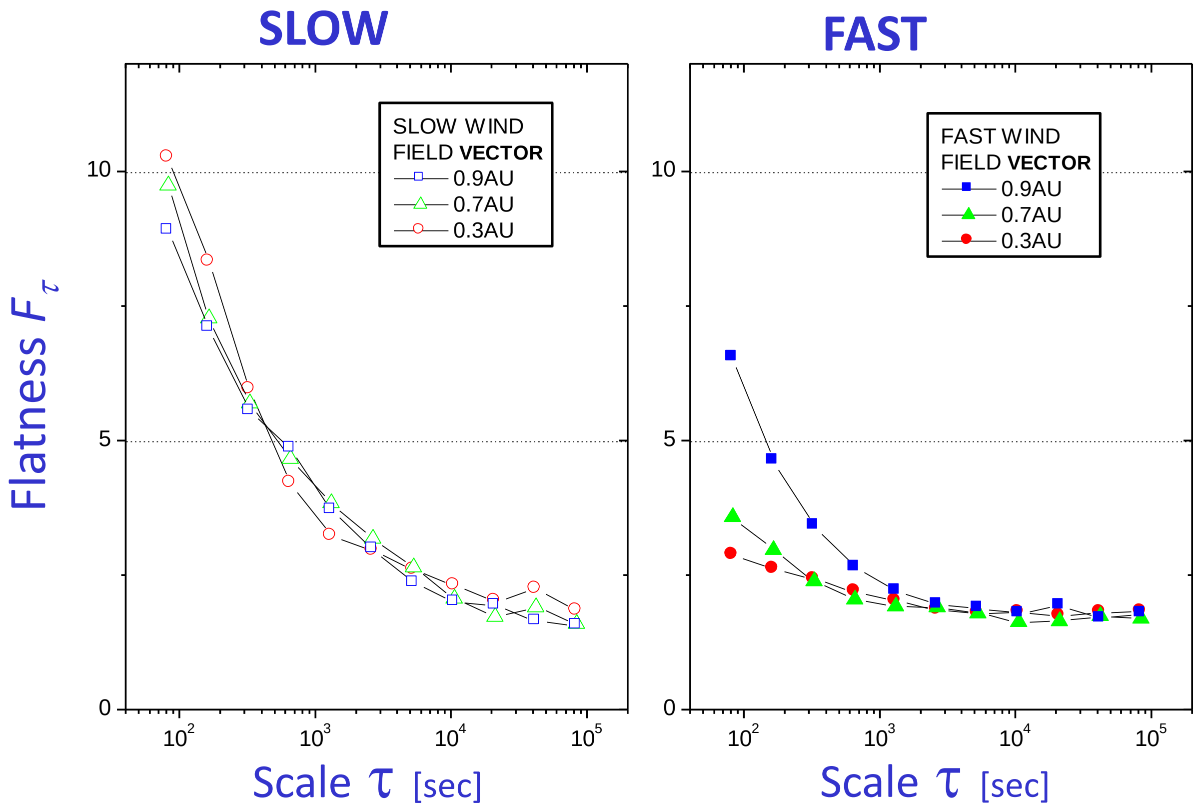

- slow wind is more intermittent than fast wind
- fast wind shows a clear radial trend which is missing in the slow wind.

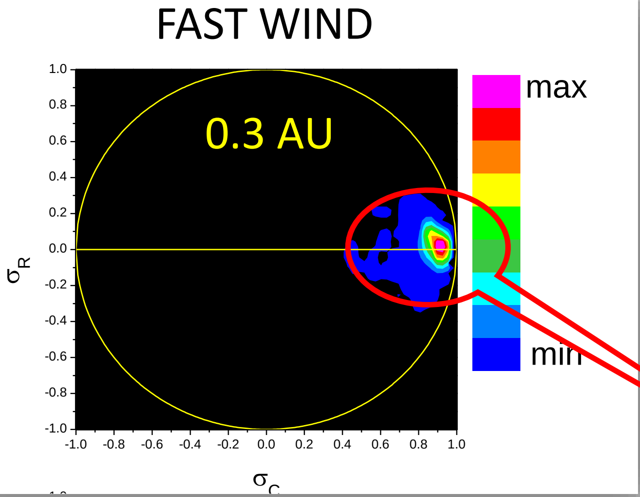

Radial evolution of MHD turbulence in terms of σ_R and σ_C (scale of 1hr)

Alfvénic population

$$\sigma_C = \frac{e^+ - e^-}{e^+ + e^-} = \frac{2 < v \cdot b >}{e^v + e^b}$$

$$\sigma_R = \frac{e^v - e^b}{e^v + e^b}$$

$$\sigma_C^2 + \sigma_R^2 \le 1$$

Radial evolution of MHD turbulence in terms of σ_R and σ_C (scale of 1hr)

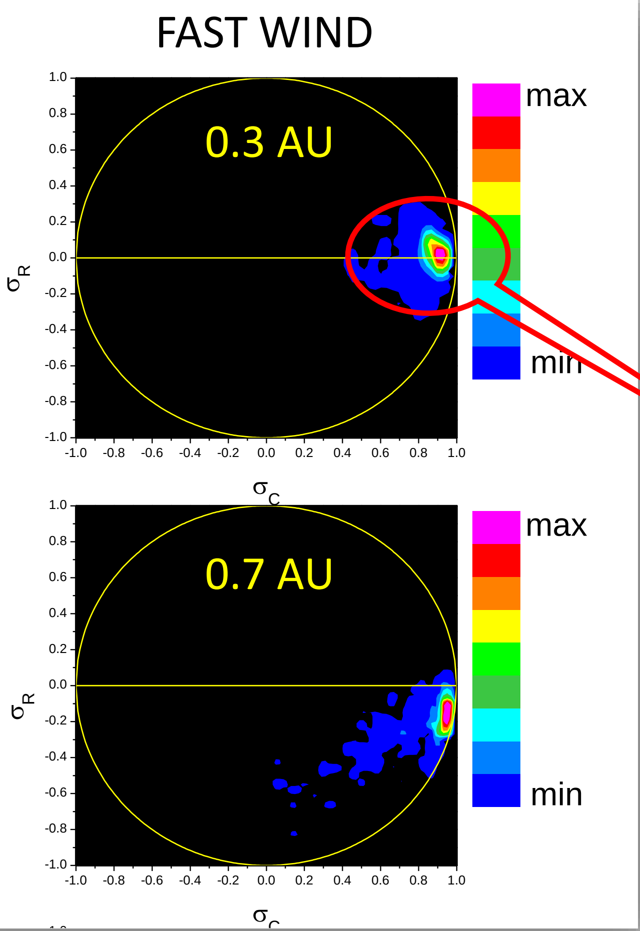

Alfvénic population

$$\sigma_C = \frac{e^+ - e^-}{e^+ + e^-} = \frac{2 < v \cdot b >}{e^v + e^b}$$

$$\sigma_R = \frac{e^v - e^b}{e^v + e^b}$$

$$\sigma_C^2 + \sigma_R^2 \le 1$$

Radial evolution of MHD turbulence in terms of σ_R and σ_C (scale of 1hr)

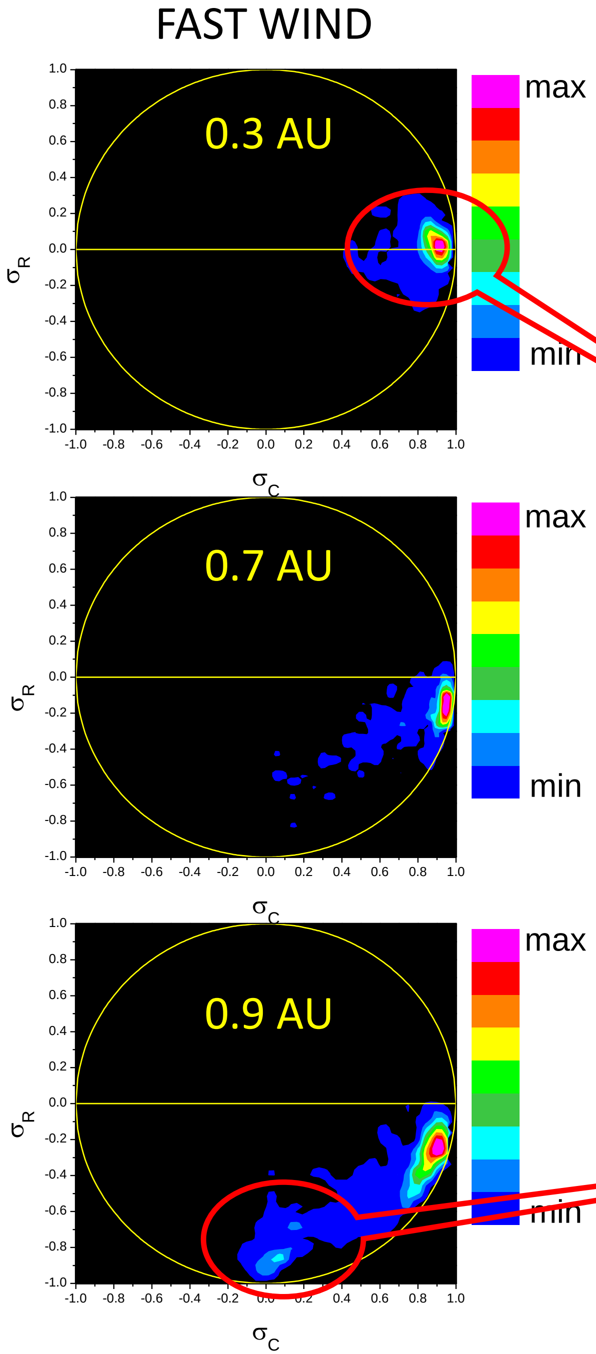

(Bruno et al., 2007)

Alfvénic population

$$\sigma_C = \frac{e^+ - e^-}{e^+ + e^-} = \frac{2 < v \cdot b >}{e^v + e^b}$$

$$\sigma_R = \frac{e^v - e^b}{e^v + e^b}$$

$$\sigma_C^2 + \sigma_R^2 \leq 1$$

A new population appears, characterized by magnetic energy excess and low Alfvénicity

Radial evolution of MHD turbulence in terms of σ_R and σ_C (scale of 1hr)

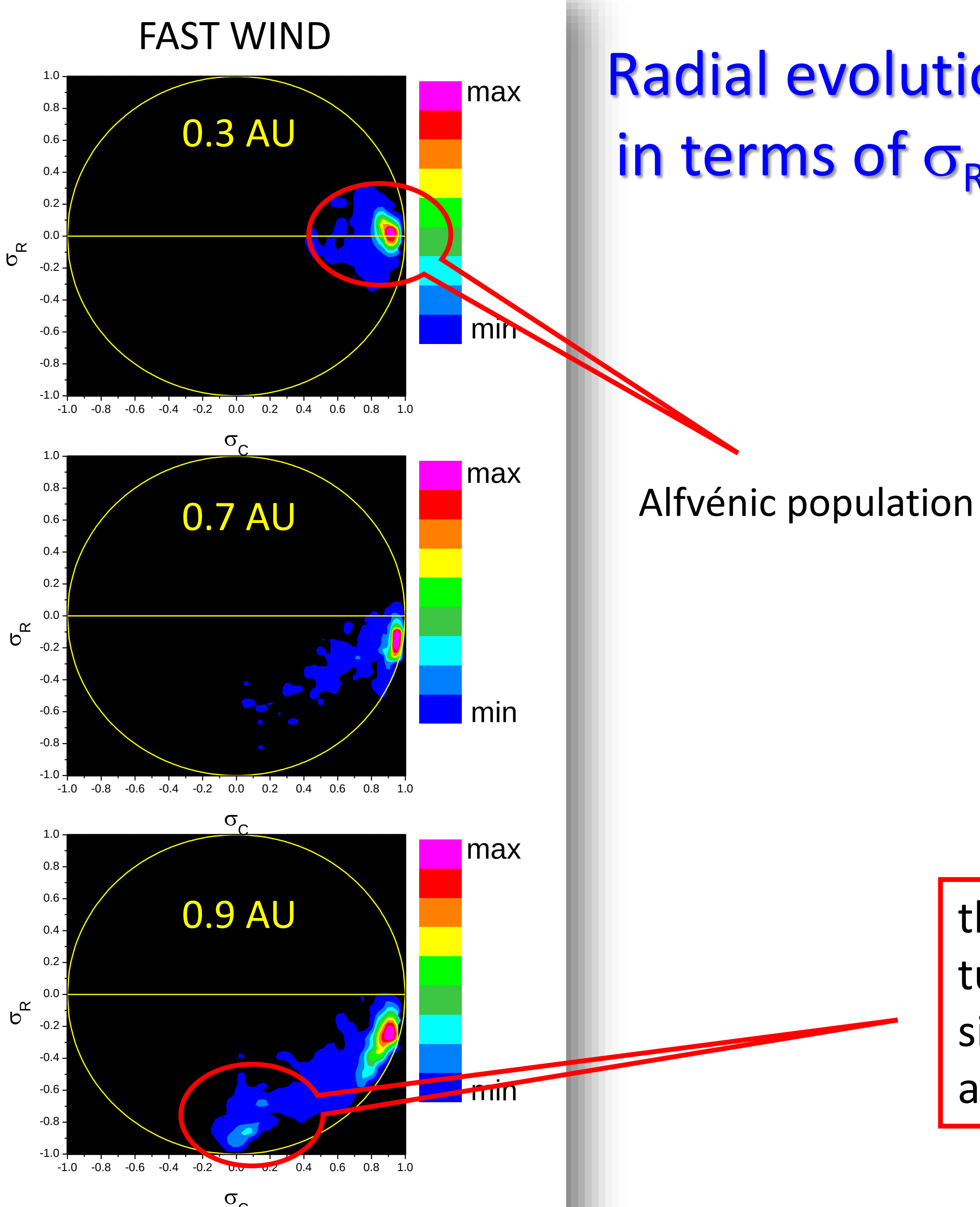

(Bruno et al., 2007)

$$\sigma_C = \frac{e^+ - e^-}{e^+ + e^-} = \frac{2 < v \cdot b >}{e^v + e^b}$$

$$\sigma_R = \frac{e^v - e^b}{e^v + e^b}$$

$$\sigma_C^2 + \sigma_R^2 \leq 1$$

this might be a result of turbulence evolution or the signature of underlying advected structure

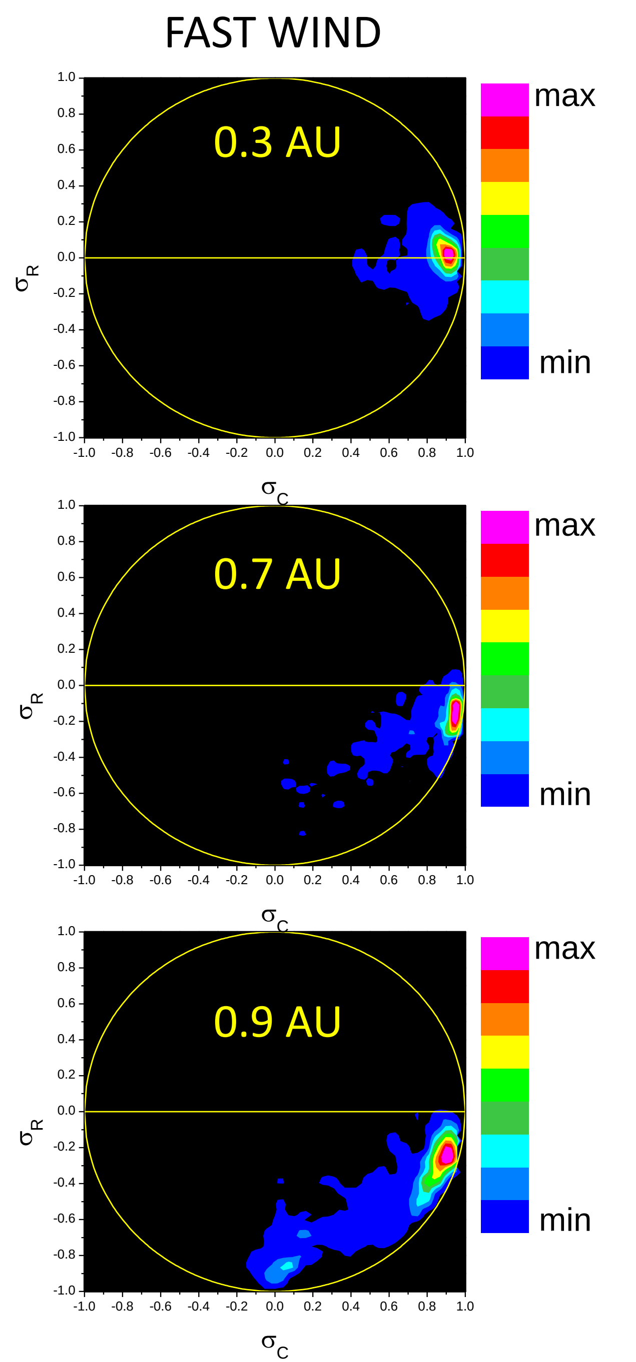

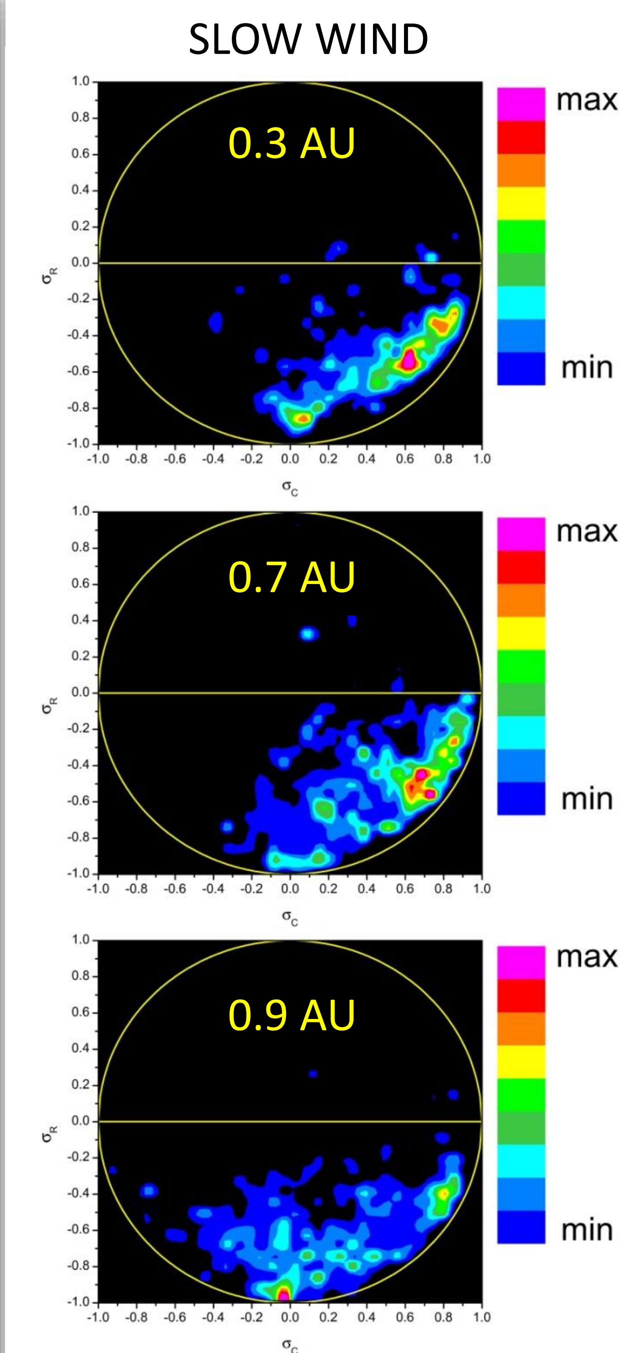

Helios 2 observations

Different situation in Slow Wind:

- no evolution
- second population already present at 0.3 AU

Solar wind turbulence is mainly made of two 'ingredients'

(Mariani et al., 1973; Thieme et al., 1988, 1989; Tu et al., 1989, 1997; Tu and Marsch, 1990, 1993; Bieber and Matthaeus, 1996; Crooker et al., 1996; Bruno et al., 2001, 2003, 2004; Chang and Wu, 2002; Chang, 2003; Chang et al., 2004; Tu and Marsch, 1992, Chang et al., 2002, Borovsky, 2006, 2009, Li, 2007, 2008, *Tu and Marsch*, 1991; *Bruno and Bavassano*, 1991, *Bieber et al*, 1996; see more refs. in *Bruno and Carbone*, 2013)

- Alfvénic fluctuations which propagate
- Structures advected by the wind or locally generated

Alfvénic fluctuations would cluster within adjacent flux-tubes along the local magnetic field direction

(*Tu and Marsch*, 1995)

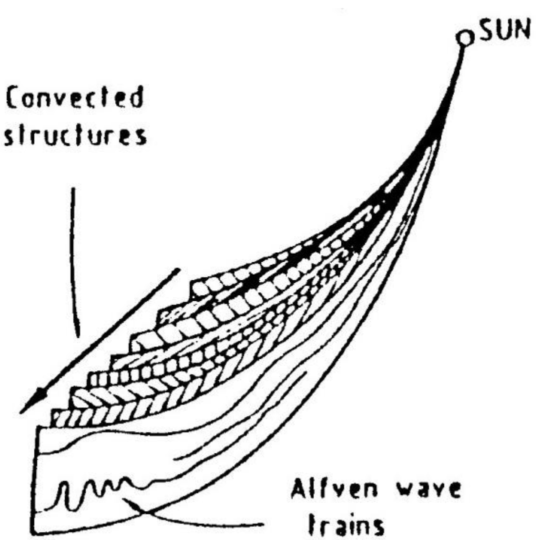

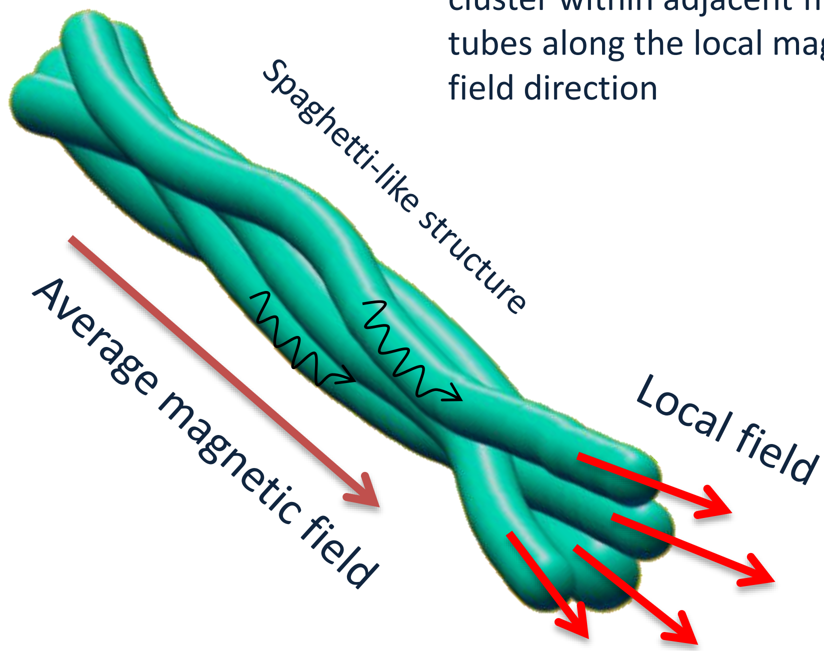

(Bruno et al, 2001)

Solar wind turbulence is mainly made of two 'ingredients'

(Mariani et al., 1973; Thieme et al., 1988, 1989; Tu et al., 1989, 1997; Tu and Marsch, 1990, 1993; Bieber and Matthaeus, 1996; Crooker et al., 1996; Bruno et al., 2001, 2003, 2004; Chang and Wu, 2002; Chang, 2003; Chang et al., 2004; Tu and Marsch, 1992, Chang et al., 2002, Borovsky, 2006, 2009, Li, 2007, 2008, *Tu and Marsch*, 1991; *Bruno and Bavassano*, 1991, *Bieber et al*, 1996; see more refs. in *Bruno and Carbone*, 2013)

- Alfvénic fluctuations which propagate
- Structures advected by the wind or locally generated

Path followed by the tip of the magnetic field vector in ~1hr

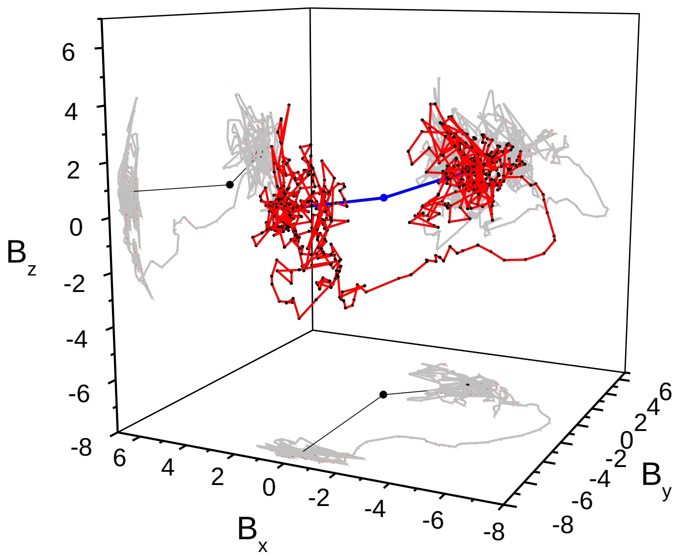

Helios 2, 6sec, 49.628-49.674 (~66min)

Alfvénic fluctuations would cluster within adjacent flux-tubes along the local magnetic field direction

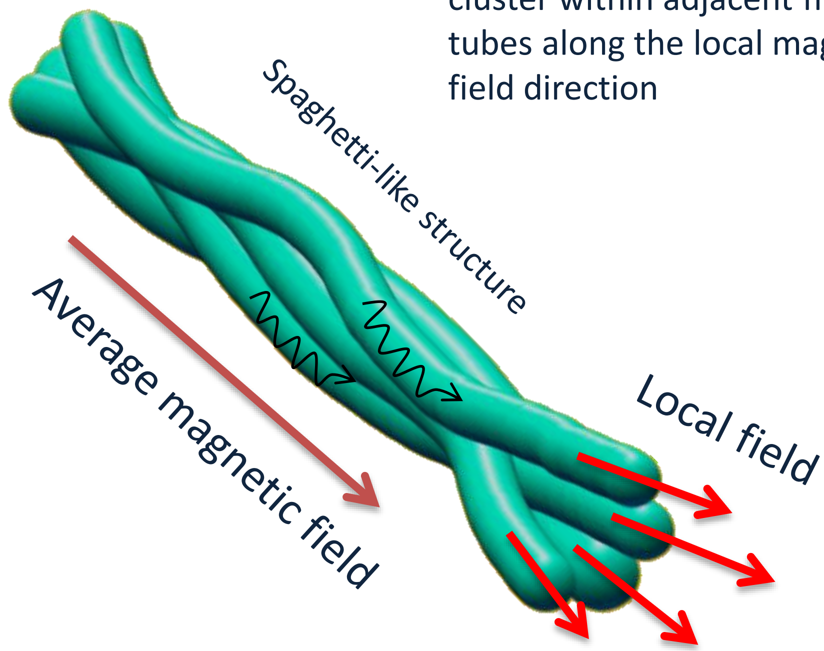

(Bruno et al, 2001)

Typical VDF and heating

(Marsch et al, 1982)

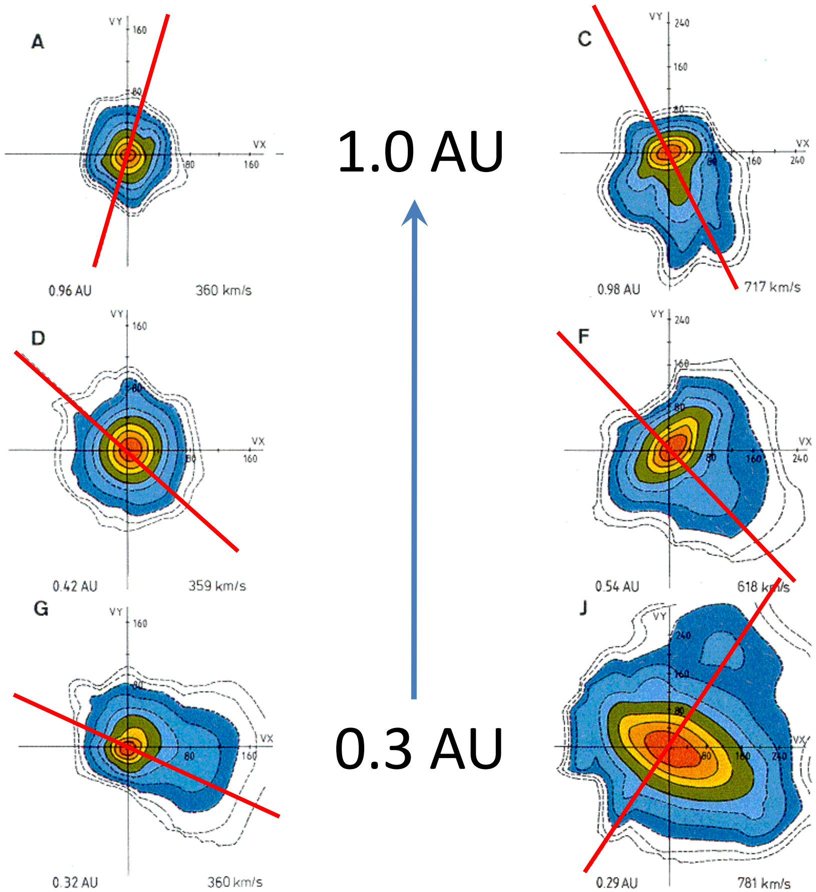

Slow wind

Fast wind

Fast wind does not expand adiabatically

Preferencial heating perpendicular to local B direction

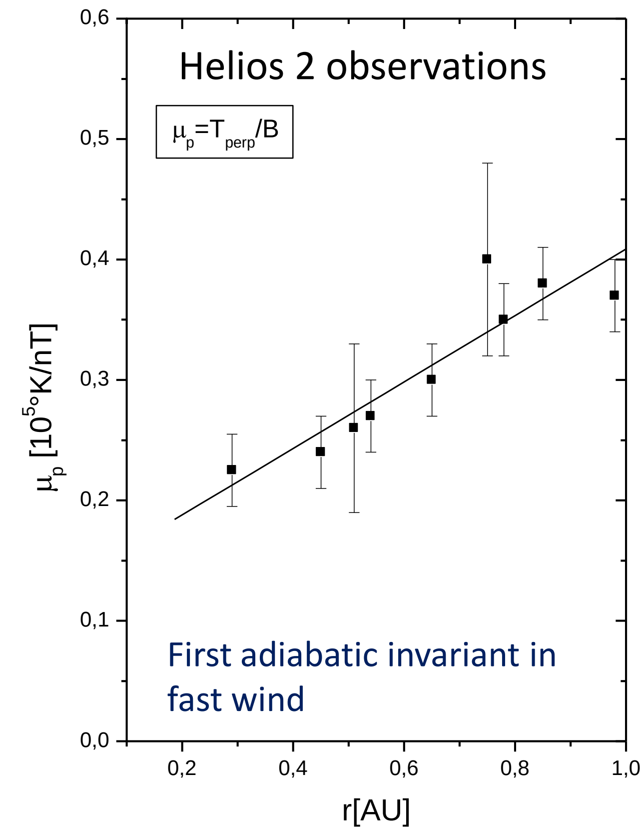

Thermal anisotropies hide kinetic processes not fully understood

Kinetic aspects

Wave-particle interactions are the key to understand ion kinetics in the corona and solar wind

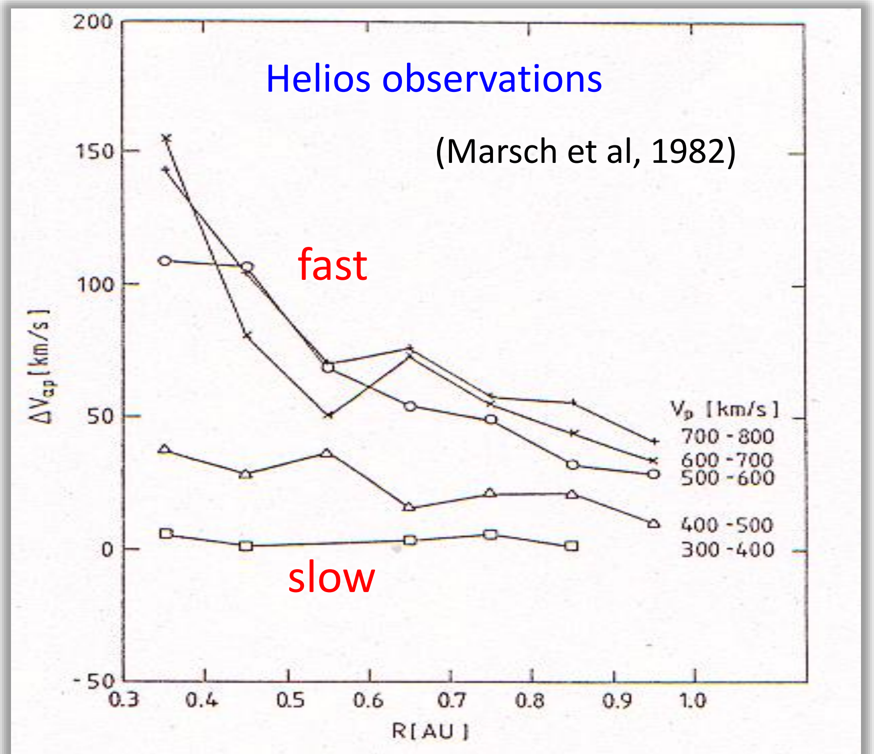

Alfvénic fluctuations might play an important role in determining the speed of minor ions.

- $\Delta V_{\alpha p}$ increases with V_{SW}
- $\Delta V_{\alpha p}$ increases approaching the sun
- $\Delta V_{\alpha p}$ is of the order of V_A
- No radial dependence for slow wind

Shaping of the proton VDF by ion-cyclotron resonance caused by Alfvén-cyclotron waves

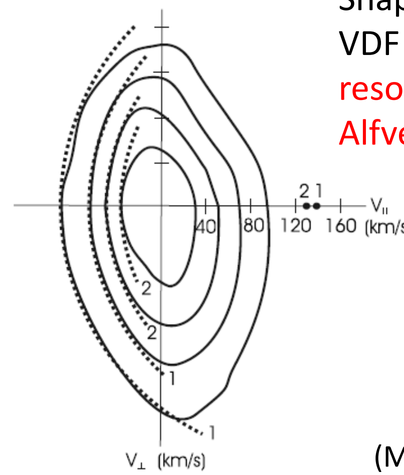

(Marsch and Tu, 2001)

ions in resonance with transverse ion-cyclotron waves, propagating parallel to the magnetic field, undergo merely pitch-angle diffusion which shapes the VDF

Radial evolution of solar wind turbulence

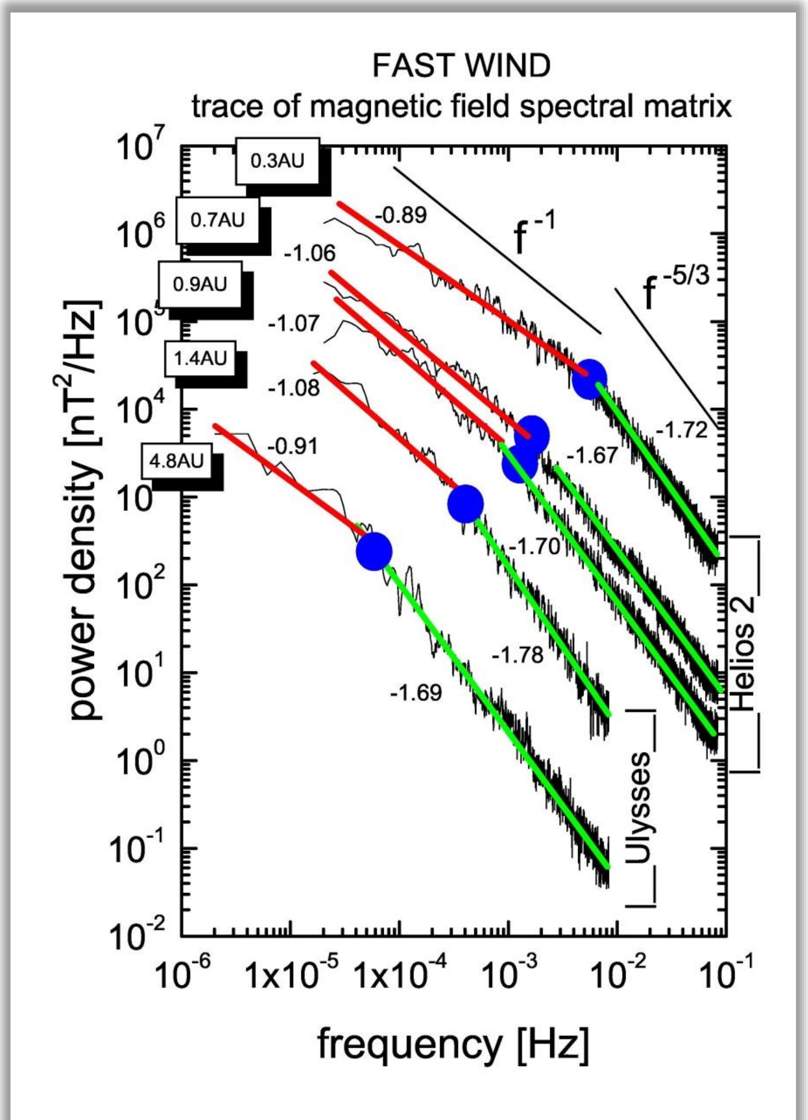

[Bruno & Carbone, 2013]

No dissipation range with Helios data since temporal resolution does not allow to investigate this range.

Radial evolution of the 'kinetic' break

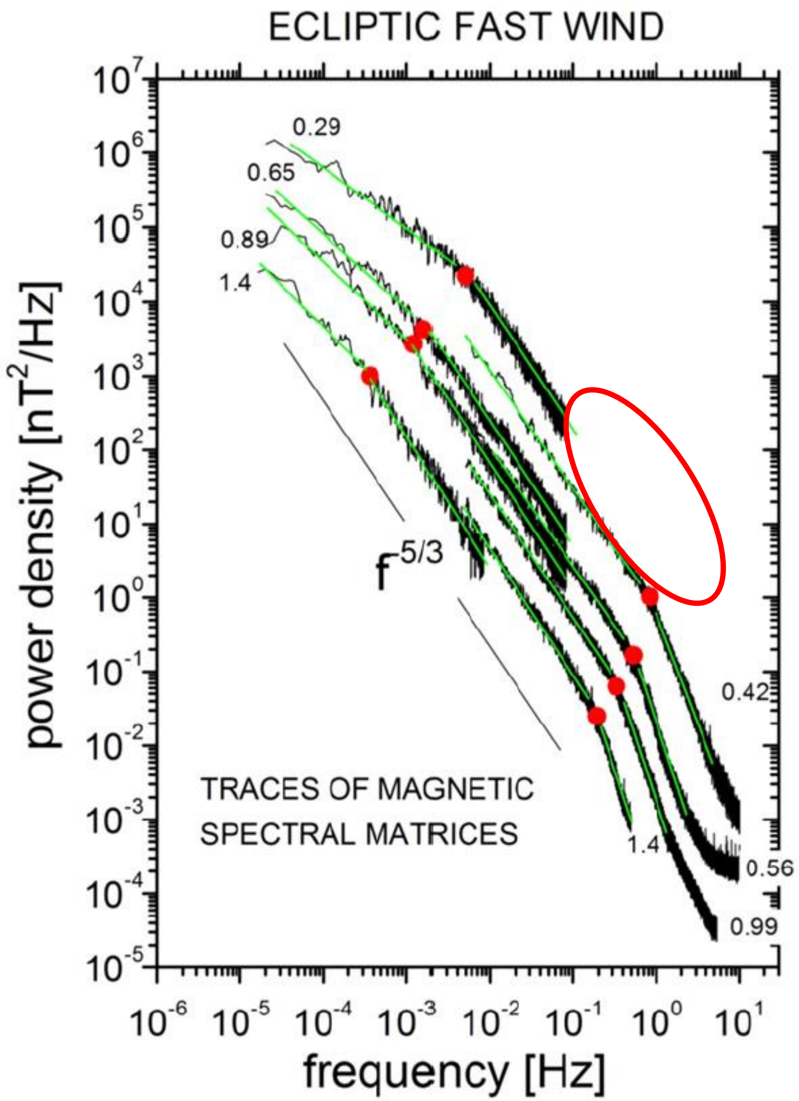

Magnetic field spectral densities relative to measurements recorded by Messenger (at 0.42 and 0.56 AU), Helios 2 (at 0.29, 0.65 and 0.89 AU), Wind at the Lagrangian point L1, and Ulysses at 1.4 AU within high-speed streams observed in the ecliptic.

Recently, it has been found that the break position is in remarkable agreement with the ion-cyclotron resonant frequency condition.

Different relevant lengths can be associated with the heating phenomenon, depending on the particular dissipation mechanism we consider.

(Telloni et al, ApJ 2015)

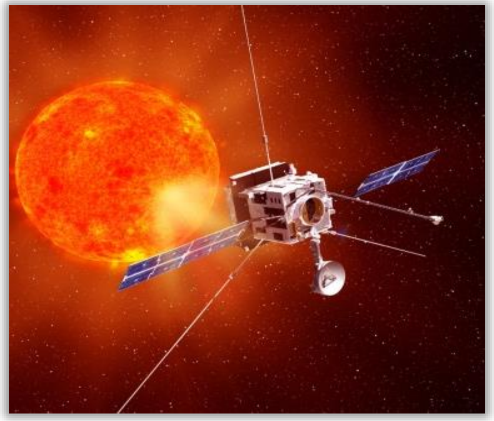

Solar Orbiter's novelties respect to previous missions

Solar Orbiter will be the first spacecraft since Helios to sample the inner heliosphere at distances as close to the Sun as 60 R_S. The main goal is to study the link between solar sources and in situ measurements. To do that:

- ✓ It will be equipped with in-situ instruments significantly more capable than those flown on Helios, as well as with remote-sensing instruments for the observation of the corona and photosphere.
- ✓ Its orbital design allows the spacecraft to achieve approximate co-rotation with the Sun for periods of several days, measuring the solar wind plasma and magnetic field in-situ while simultaneously observing their source regions on the Sun.
- ✓ Increasing inclination up to more than 30° with respect to the solar equator allows out-of-ecliptic measurements.

SolO's orbit

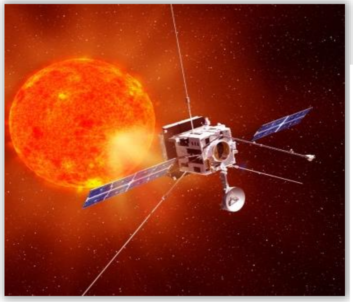

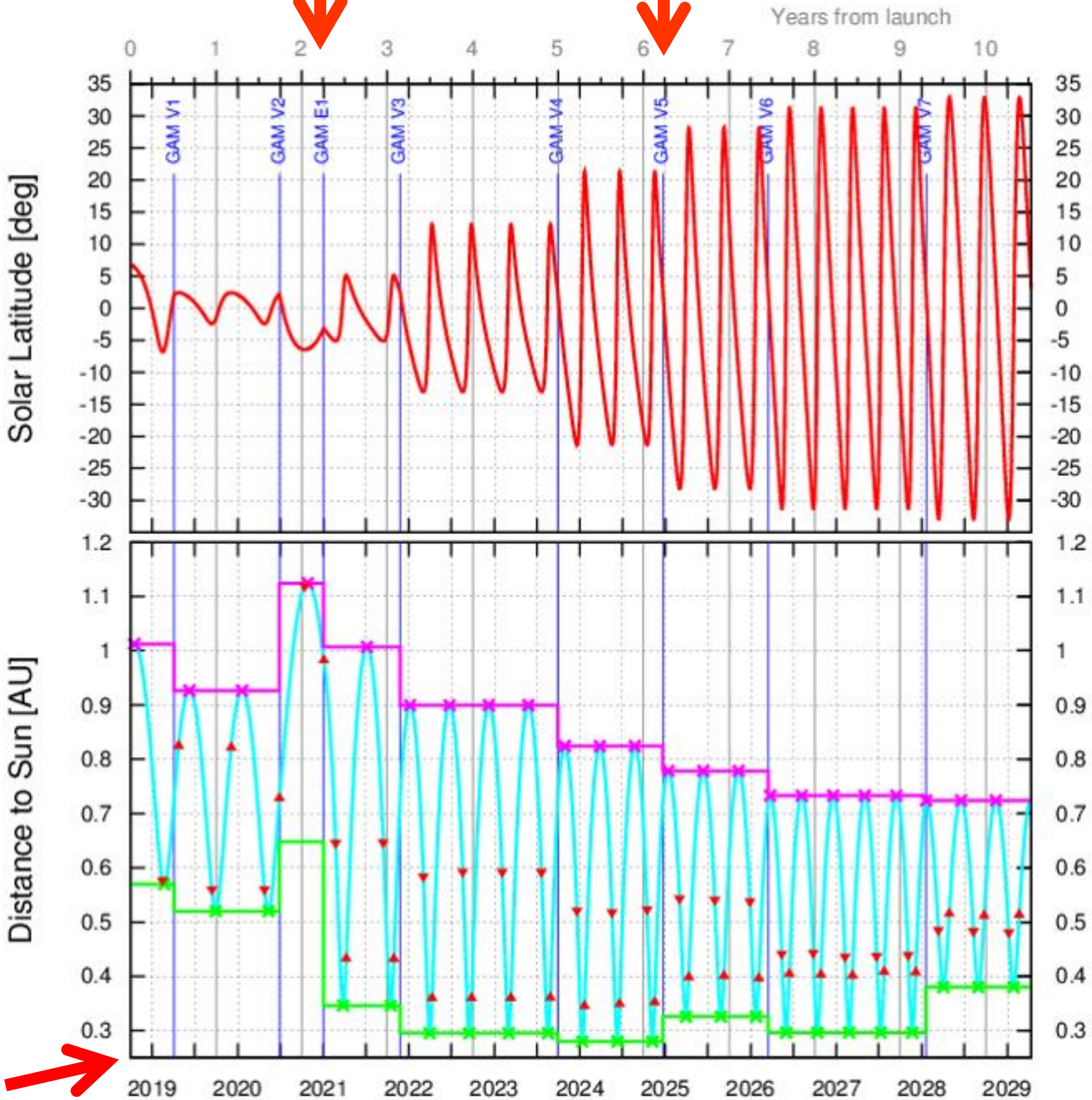

October 2018

Cruise Nominal Extended

Solar Orbiter detailed science objectives

Objective 1: What drives the solar wind and where does the heliospheric magnetic field originate?

1.1 What are the source regions of the solar wind and heliospheric magnetic field?
1.2 What mechanisms heat and accelerate the solar wind?
1.3 What are the sources of solar wind turbulence and how does it evolve?

Objective 2: How do solar transients drive heliospheric variability?

2.1 How do CMEs evolve through the corona and inner heliosphere?
2.2 How do CMEs contribute to solar magnetic flux and helicity balance?
2.3 How and where do shocks form in the corona?

Objective 3: How do solar eruptions produce energetic particle radiation that fills the heliosphere?

3.1 How and where are energetic particles accelerated at the Sun?
3.2 How are energetic particles released from their sources and distributed in space and time?
3.3 What are the seed populations for energetic particles?

Objective 4: How does the solar dynamo work and drive connections between the Sun and the heliosphere?

4.1 How is magnetic flux transported to and re-processed at high solar latitudes?
4.2 What are the properties of the magnetic field at high solar latitudes?
4.3 Are there separate dynamo processes acting in the Sun?

Payload: In-Situ Instruments

EPD	Energetic Particle Detector	J. Rodríguez-Pacheco(E)	Composition, timing and distribution functions of energetic particles
MAG	Magnetometer	T. Horbury (UK)	High-precision measurements of the heliospheric magnetic field
RPW	Radio & Plasma Waves	M. Maksimovic (F)	Electromagnetic and electrostatic waves, magnetic and electric fields at high time resolution
SWA	Solar Wind Analyser	C. Owen (UK)	Sampling protons, electrons and heavy ions in the solar wind

Payload: Remote-Sensing Instruments

EUI	Extreme Ultraviolet Imager	P. Rochus (B)	High-resolution and full-disk EUV imaging of the on-disk solar corona
METIS	Coronagraph	E. Antonucci (I)	Visible and (E)UV imaging of the off-disk corona
PHI	Polarimetric & Helioseismic Imager	S. Solanki (D)	High-resolution vector magnetic field, line-of-sight velocity in photosphere, visible imaging
SoloHI	Heliospheric Imager	R. Howard (USA)	Wide-field visible imaging of the solar corona and wind
SPICE	Spectral Imaging of the Coronal Environment	European-led	EUV spectroscopy of the solar disk and near-Sun solar corona
STIX	Spectrometer/Telecope for Imaging X-rays	S. Krucker (CH)	Imaging spectroscopy of solar X-ray emission

Solar Wind Analyser Plasma Suite

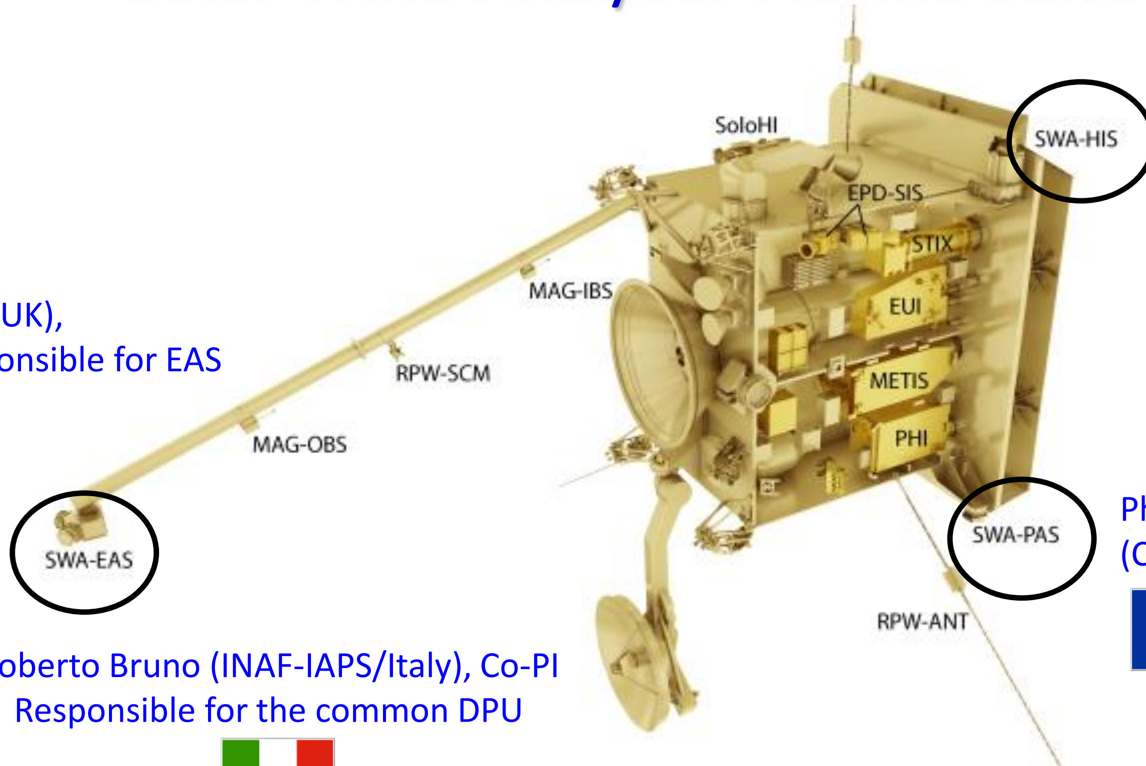

Stefano Livi
(SwRI/USA), Co-PI

Chris Owen (MSSL/UK),
PI of SWA and responsible for EAS

Philippe Louarn
(CESR/France), Co-PI

Roberto Bruno (INAF-IAPS/Italy), Co-PI
Responsible for the common DPU

The Solar Wind Plasma Analyzer (SWA) consists of a suite of 3 sensors:

- the Electron Analyser System (EAS),
- the Proton-Alpha Sensor (PAS) and
- the Heavy Ion Sensor (HIS),

together with a common DPU.

First suite of coordinated in situ measurements made inside 1 AU, which include <u>mass composition</u> as well as <u>high resolution 3-D velocity distributions</u> (ions and electrons).

Proton and Alpha Sensor (PAS)

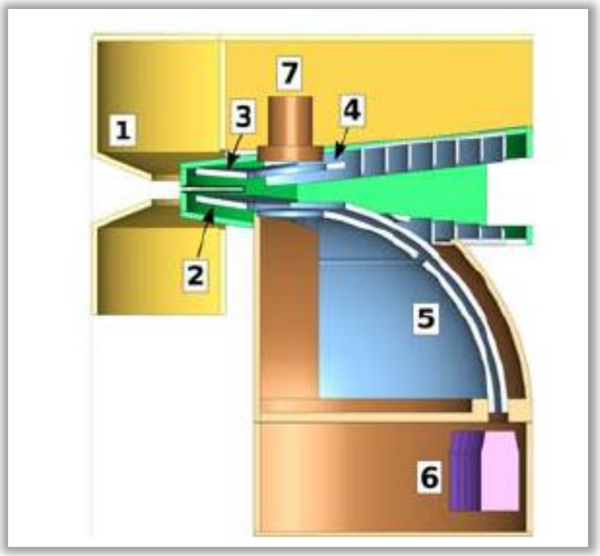

- Energy range from 0.2 – 20 keV/q, with $\Delta E/E$ ~7.5%
- FoV: elevation ±22.5° $\Delta\Theta$ = 5 °, azimuth -24° ÷ 42° $\Delta\Phi$ = 6°

High temporal resolution

- **Full 3D VDF** sampled at 1 sec (NM)
- **Moments** (number density, bulk speed, pressure tensor) of the proton distribution at 4s (NM)
- Reduced 3-D distributions up to 14 Hz (BM)

Scientific objectives

- kinetic and fluid properties of the bulk solar wind plasma and dominant physical processes (e.g.: wave- particle interactions, origin and dissipation of turbulence, etc);
- dynamics and evolution of stream interactions, shocks and CMEs

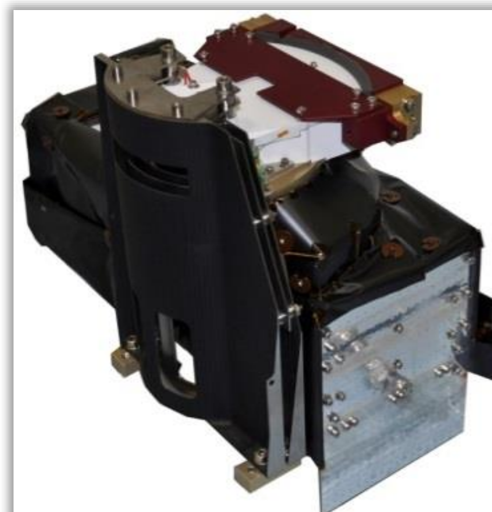

HELIOS-Solar Orbiter comparison

SWA:

- sampling capabilities three orders of magnitude faster than Helios.
- First time exploration of the dissipation range with 3D VDF

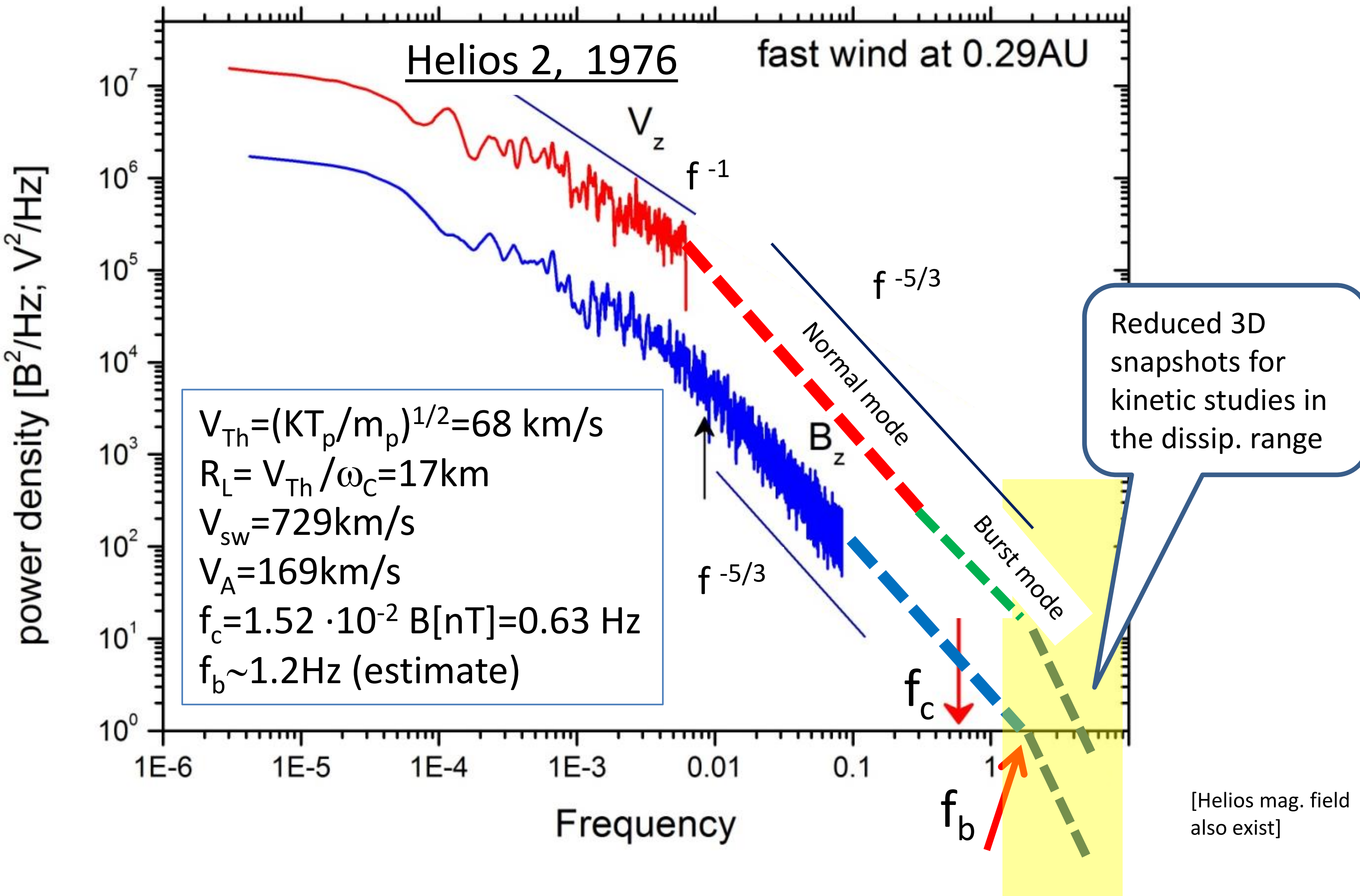

[Helios mag. field @ 4Hz also exist]

Structures advected by the wind

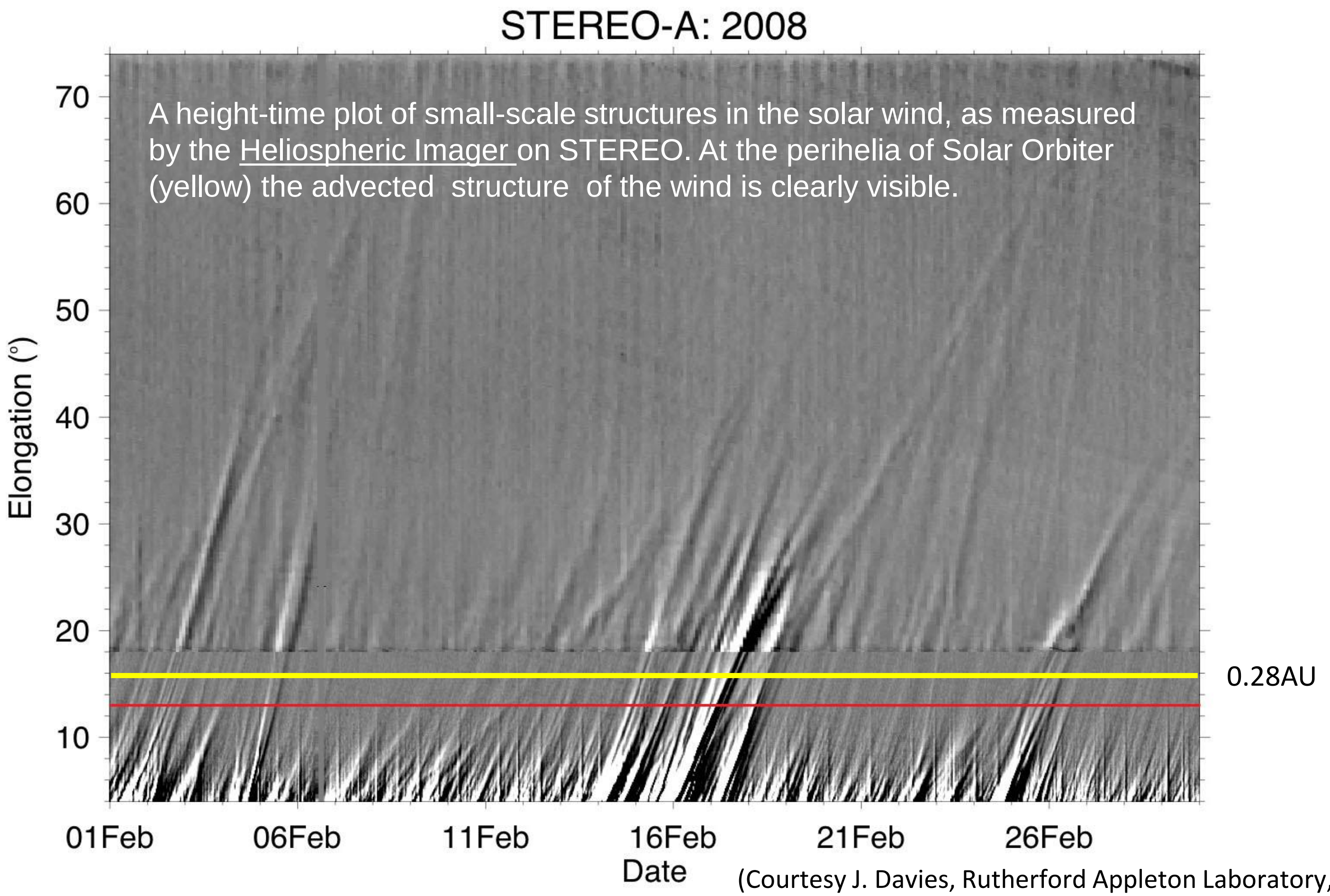

(Courtesy J. Davies, Rutherford Appleton Laboratory, UK)

Going close to the sun and sampling for long enough time intervals will allow to go through the advected structure of the wind

Conclusion

- ✓ Helios still represents a unique dataset to study the radial evolution of solar wind fluctuations in the inner heliosphere
- ✓ Our scientific community has been working with Helios data for the past 40 years mainly using data from the primary missions of Helios 1 and 2 (about 4 months each), publishing hundreds of papers.

- SolO is a discovery mission: remote & in situ packages @ 0.28 AU, corotation, high latitude
- SolO will answer fundamental questions relevant to both solar and stellar physics.
- The Solar Wind Analyser will investigate kinetic and fluid properties of the bulk solar wind plasma and dominant physical processes allowing to investigate for the first time composition and the dissipation range close to the Sun.

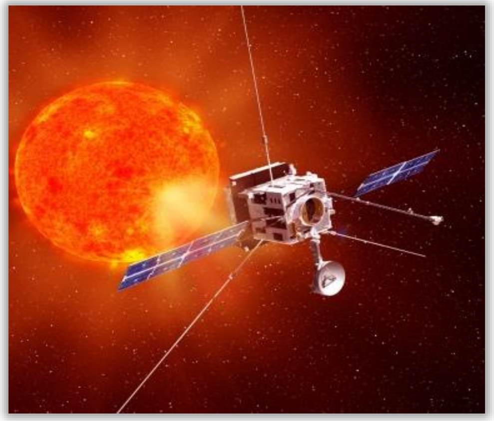

The spectral cascade ends up in what looks like a "dissipation range "

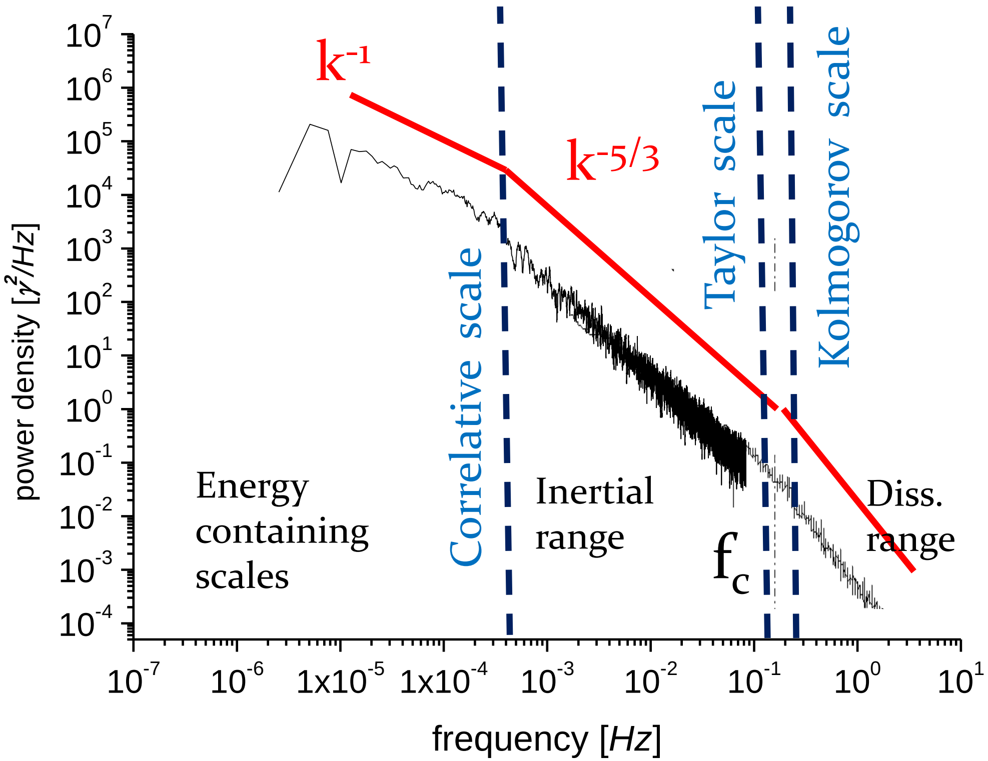

typical IMF power spectrum in at 1 AU

[Low frequency from Helios (Bruno et al., 1985), high freq. tail from WIND (Leamon et al, 1998)]

- Correlative Scale/Integral Scale:
  - the largest separation distance over which eddies are still correlated. i.e. the largest turb. eddy size.
- Taylor scale:
  - The scale size at which viscous dissipation begins to affect the eddies.
  - Several times larger than Kolmogorov scale
  - it marks the transition from the inertial range to the dissipation range.
- Kolmogorov scale:
  - The scale size that characterizes the smallest dissipation-scale eddies

$$\boxed{R_m = \left(\frac{\lambda_C}{\lambda_T}\right)^2}$$

(Batchelor, 1970)

- different relevant lengths can be associated with the heating phenomenon, depending on the particular dissipation mechanism we consider

- Characteristic scales which could be related to the observed spectral break are:

Proton inertial length $\lambda_i = 2\pi c / \omega_p$

Proton Larmor radius $\lambda_L = 2\pi v_{th} / \Omega_p$

where

$\omega_p = \left(4\pi n q^2 / m_p\right)^{1/2}$ proton plasma frequency [rad/s]

$\Omega_p = qB / \left(m_p c\right)$ proton cyclotron frequency [rad/s]

since $c / \omega_p = v_A / \Omega_p$

proton inertial length can be expressed as $\lambda_i = 2\pi v_A / \Omega_p \Longrightarrow \lambda_i \cong \lambda_L$

Heavy ions will help to identify the source regions of CME's

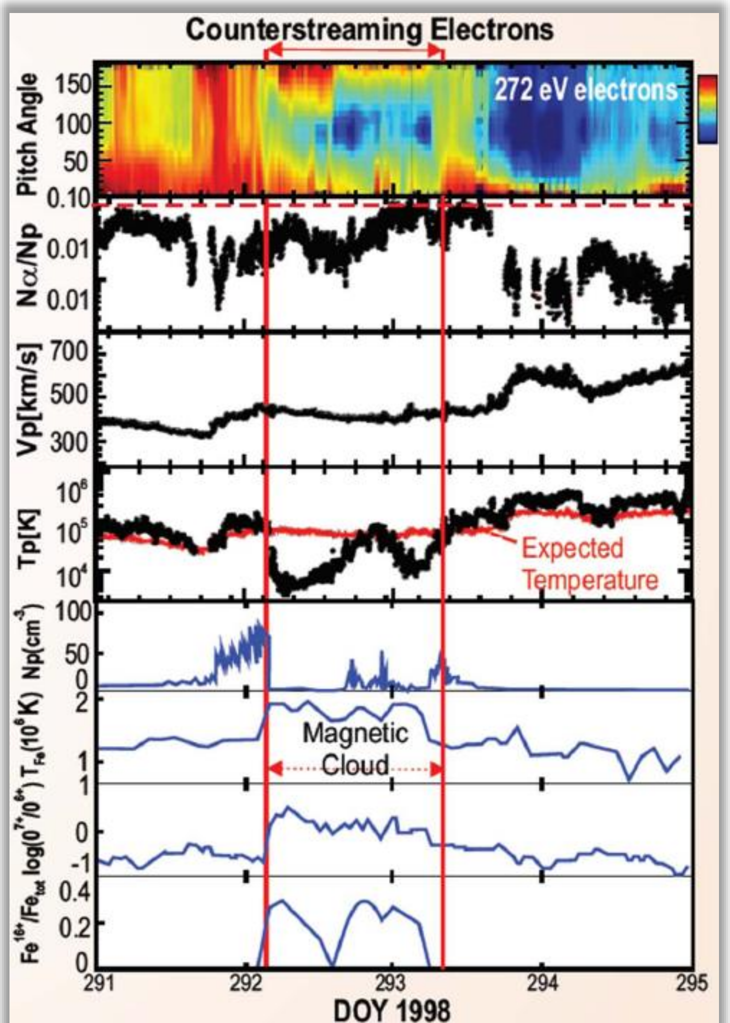

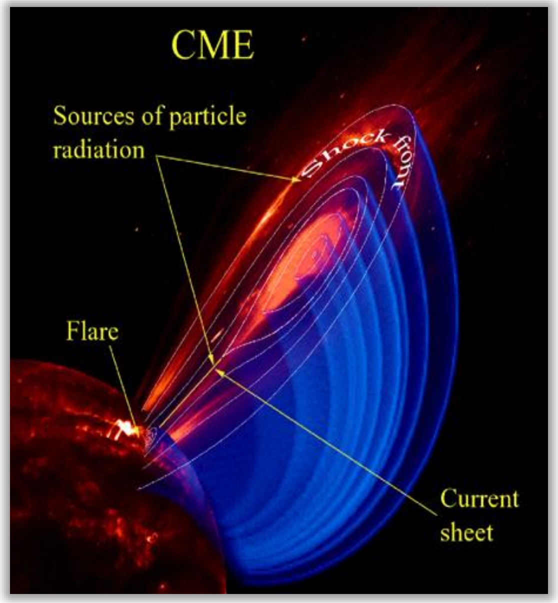

SWA measurements of
- electron pitch angle distribution,
- alpha/proton ratio,
- freeze-in temperature (e.g. Fe),
- O and Fe charge state ratios

will establish firm links between coronal sources of CME's and their in-situ counterparts.

Origin of the solar wind

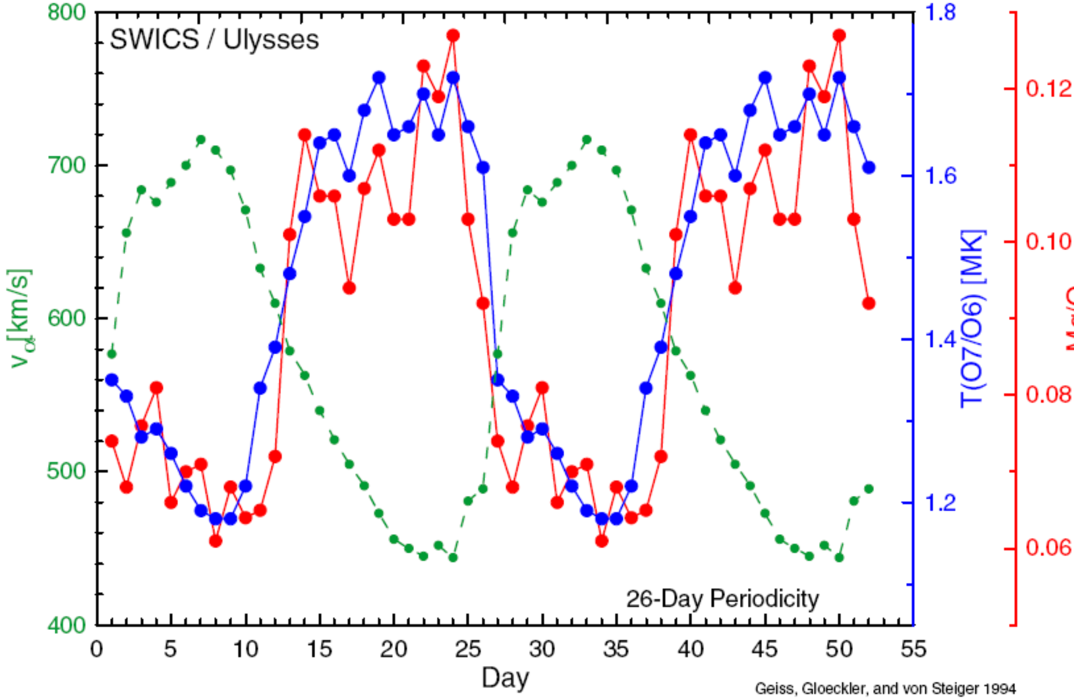

The transition between fast and slow wind is sharply detected by elemental and charge composition which remains unchanged during wind expansion.

Small scale properties of coronal hole boundaries can be detected

TABLE I. A list of the most abundant elements present in the solar photosphere arranged according to their FIP.

Element	Z	FIP (eV)	Photospheric abundance (relative to H)
He	2	24.6	9.0×10^{-2}
Ne	10	21.6	1.2×10^{-4}
Ar	18	15.8	3.6×10^{-6}
N	7	14.5	1.1×10^{-4}
H	1	13.6	1
O	8	13.6	8.5×10^{-4}
Cl	17	13.0	1.9×10^{-7}
C	6	11.3	3.6×10^{-4}
P	15	10.5	3.7×10^{-7}
S	16	10.3	1.9×10^{-5}
Si	14	8.1	3.6×10^{-5}
Fe	26	7.9	3.2×10^{-5}
Mg	12	7.6	3.8×10^{-5}
Ni	28	7.6	1.8×10^{-6}
Mn	25	7.4	3.4×10^{-7}
Cr	24	6.8	4.8×10^{-7}
Ca	20	6.1	2.2×10^{-6}
Al	13	6.0	3.0×10^{-6}
Na	11	5.2	2.1×10^{-6}
K	19	4.3	1.4×10^{-7}

Slow wind has higher oxygen freeze-in temperature
Slow wind has higher FIP effect (enrichment of Mg/O, Mg has a lower FIP with respect to O)

Power law spectra → self-similarity

A typical IMF power spectrum in interplanetary space at 1 AU [Low frequency from *Bruno et al*., 1985; high freq. tail from *Leamon et al*, 1999]

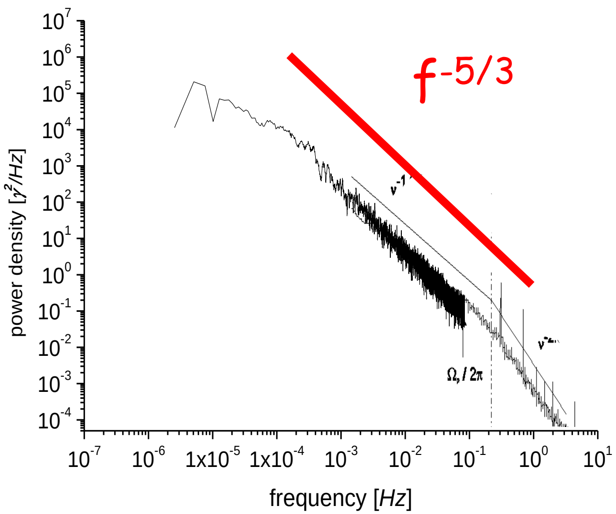

Power law brings scale invariance

A given observable $v(\ell)$ is invariant for a scale transformation $\ell \to r\ell$ if there exists a parameter $\mu(r)$ such that $v(\ell)=\mu(r)v(r\ell)$. The solution of this relation is a power law: $v(\ell)=C\ell^h$ where $h=\log \mu(r)$.

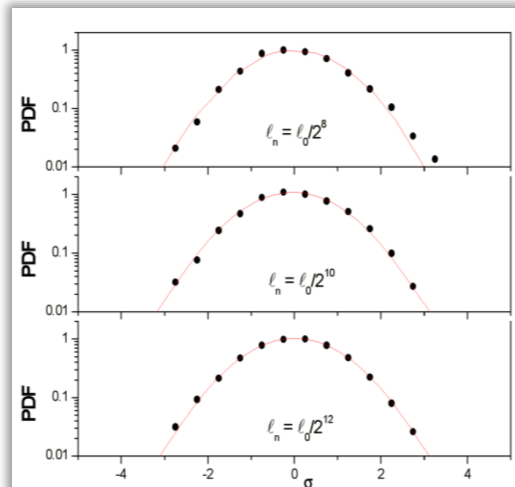

(numerical simulations)

From small to large scales

Scale invariance implies self-similar PDFs

If we introduce a scale transformation $\ell \to r\ell$, we obtain: $\delta v_{r\ell} \sim r^h \delta v_\ell$ that implies that $PDF(\delta v_{r\ell}) \sim PDF(r^h \delta v_\ell)$.

Van Atta and Park (1975) showed that, using standardized variables like $y_\ell = \delta v_\ell / \left\langle (\delta v_\ell)^2 \right\rangle^{1/2}$, we obtain:

$PDF(y_\ell)=PDF(y_{r\ell})$.